Innovative Infrastructure Solutions (2022) 7: 305
https://doi.org/10.1007/s41062-022-00907-8

TECHNICAL PAPER

Implementation assessment of calcined and uncalcined cashew nut-shell ash with total recycled concrete aggregate in self-compacting concrete employing Bailey grading technique

Adithya Tantri[1] · Gopinatha Nayak[1] · Adithya Shenoy[1] · Kiran K. Shetty[1] · Jagadisha Achar[1] · Muralidhar Kamath[1]

Received: 21 May 2022 / Accepted: 25 July 2022 / Published online: 13 August 2022

Abstract

The present study concentrates on the performance evaluation of calcined and uncalcined cashew nut-shell ash (UCCNA and CCNA) with treated total recycled concrete aggregate (TRCA) in self-compacting concrete. The achievement of sustainable self-compacting concrete (SCC) is possible by the implication of four stages, which includes TRCA treatment process, gradation selection process through Bailey aggregate grading technique, by considering TRCA replacement percentage with an increment of 25% and up to 100% and by considering UCCNA or CCNA replacement with an increment of 5% and up to 20%. Hardened and fresh properties of SCC have been performed and analyzed based on the compliance requirements of SCC. In addition finding results through microstructure assessment was in line with the findings of the hardened and fresh properties of SCC. In addition, quality and dynamic instability assessments of SCC were analyzed through ultrasonic pulse velocity and drying shrinkage aspects. Besides CO_2, the emission rate and the efficiency rate of SCC, composites were analyzed in detail. Overall findings revealed that CCNA-based SCC mixes performed effectively than UCCNA-based SCC; specifically, incorporation of 75% of TRCA with 15% CCNA was found to be optimal. But with regard to shrinkage performance UCCNA found to be better by imputing less shrinkage compared to CCNA-based SCC mixes. Further with regard to efficiency rate of SCC composites revealed the gain of maximum efficiency of about 0.156 MPa/kg CO_2/m^3 and 0.160 MPa/kg CO_2/m^3 for 15% and 20% CCNA-based SCC mixes.

Keywords Self-compacting concrete · Microstructure · Drying shrinkage · Bailey gradation · Concrete efficiency · CO_2 emission

Introduction

Utilization of agro-waste materials as cementitious or pozzolanic in versatile concrete was found to be more frequent. Most utilized agro-wastes in concrete are rice husk ash, bagasse, groundnut shell ash, oyster shell ash, sawdust ash, and cork waste ash [1–3]. Most of these agro-wastes must undergo a calcination process, which results in property enhancement [2, 4, 5]. Usually, these processes were executed at a higher temperature of about 400–800 °C depending on the agro-waste nature [2, 4, 6, 7]. However, in the perceptive of time dependency, energy consumption and environmental benefits make the final product less sustainable [8, 9]. Developing countries like India, which is the third-largest producer of cashew nut in the world, perform disposal of cashew nut-shell with an uncontrolled burning technique [10, 11]. These under-burnt cashew nut-shells (< 400 °C)

✉ Adithya Tantri
aditya.tantry001@gmail.com

✉ Gopinatha Nayak
nayak.gopinath@manipal.edu

✉ Muralidhar Kamath
Muralidhar.kamath@learner.manipal.edu

Adithya Shenoy
adithya.shenoy@learner.manipal.edu

Kiran K. Shetty
kiran.shetty@manipal.edu

Jagadisha Achar
jaga.disha007@gmail.com

[1] Department of Civil Engineering, Manipal Institute of Technology, Manipal Academy of Higher Education, Manipal, Karnataka 576104, India

produce un-calcined cashew nut-shell ash (UCCNA) with more unburnt carbons [12]. Calcined (400–800 °C) cashew nut-shell ash (CCNA) produces whitish and greyish particles which is the representation of crystallization of silica [12, 13]. Literature reveals about two types of CCNA which are bifurcated as CaO-based CCNA (35.67% max) and SiO_2-based CCNA (62.85% max) [12–15]. These two CCNA variants impart diverse nature in the fresh and hardened properties of concrete. Implication SiO_2-based CCNA with ordinary portland cement (OPC) enhances the slump flow and compaction factor properties due to the low quantification or absence of CaO, which implies retarder behaviour in cement paste at the initial state of hydration [15]. CaO-based CCNA imparts a decreasing nature in slump flow performances because the presence of high quantified CaO accelerates the hydration process in cement paste. Limited studies were executed and addressed towards the comparison of calcined and uncalcined agro-waste products on concrete applications [14]. To date, optimum utilization of CCNA is proposed up to 15%, 20%, and 25% recommended by Oyebisis et al., Thirumurugan et al., and Pandi et al., respectively [13, 15, 16]. However, to date, no study is performed on the utilization of UCCNA in concrete paste appliances. In addition, oxide nature variance of CCNA from source to source promotes the scope of research.

Aggregate is a predominant material that is used on a vast scale in the construction industry. Due to the better durability of igneous rock-based aggregates, granite and basalt are most preferred and utilized in the construction industry to date [17–19]. In India, aggregate flow analysis revealed that 99% of the produced stone is utilized in concrete, and its demand is about 1.089 billion tonnes per annum [17, 20]. The stone process has a significant impact on air pollution, not least in terms of CO_2 emissions from the use of fossil fuels and electricity [17, 18, 21]. Utilization of total recycled concrete aggregates (TRCA) in concrete is the way forward for the environmental benefits. In addition utilization of TRCA in concrete helps to mitigate the CO_2 emissions from the processing of natural stone into aggregate. Natural aggregate processing involves quarrying, crushing and transportation which leads to the production of 20 kg of CO_2/1000 kg of natural aggregates [18]. On the other hand processing of 1000 kg TRCA roughly saves 8 kg of CO_2 [18, 20]. In India, in the future, if all of the aggregates are replaced by TRCA in concrete, it will save 8 million tonnes of CO_2 per annum [17, 18]. TRCA represents the inclusion of both recycled coarse and fine aggregates, which is found to be more suitable for structural concrete because of its favourable characteristics to those of reclaimed asphalt pavement aggregates and mixed recycled aggregates [22–24]. In addition, TRCA has a crucial influential hold on concrete properties due to its adhere mortar. Its impact on the concrete property was more significant as the increase of replacement percentage [25–29]. As far as this, vast studies were carried out for concrete with coarse TRCA. Many developed nations accept the TRCA coarse as a major construction material [30]. On antithesis, very few studies have been made regards TRCA fines, and many countries do not recommend utilizing it in actual construction practices [22, 30]. It may be due to the uncertain property behaviour of TRCA fines in composite concrete. It promotes the vast study, especially from 2004 onwards many studies recommend utilizing TRCA fines in concrete with procured limitations [28, 31]. Particle packing methods have been considered as one of the procured methods to mitigate the drawbacks of TRCA on concrete performance. Bailey aggregate grading technique (BAGT) is a particle grading tool, which was initially proposed for asphalt mixes [32–34]. However, this technique was found to be most suitable for self-compacting concrete (SCC) where it was purely based on the particle orientation factor, which was necessary where it would be expected that aggregate must self-orient itself to achieve the densified compacted state [35, 36]. Further BAGT was found to be more suitable for recycled-based SCC [37]. However, to date, no study has been performed by utilizing BAGT with TRCA in SCC, and it was found to be a research scope of interest.

The application of SCC was found to be vast in the current construction industry. In addition, trial and error-based practical-oriented SCC mix design promotes research, and presently vast studies are practised [38, 39]. Pereira-de-Oliveira et al. [40] and Grdic et al. [41] studies revealed that the inclusion of TRCA in SCC slightly reduced rheology and mechanical properties. However, the study of Fakitsas et al. [42] and Khodair and Bommareddy [43] revealed that TRCA inclusion significantly promotes compressive, tensile, and shear strength of SCC. It represents the complex behaviour of TRCA in SCC, and it depends on TRCA characteristics which rely on TRCA treatment or adhere mortar quality and content. To date, several treating procedures were adopted to enhance the adhere mortar property or to reduce the adhere mortar thickness around the TRCA [44]. Mechanical grinding, selective heat grinding, heat grinding, pre-soaking water, and pre-soaking in acids were practised procedures for removing adhered mortar from TRCA [45–48]. It was observed that adaptation of these physical treatments succeeded to impart 7% more mechanical properties at the age of 28-day curing period [44]. Still, these procedures challenge the TRCA toughness, texture, and bonding characteristics which were necessary to address regards of durability aspects of concrete [49, 50]. Polymer emulsion, filler lime powder, calcium carbonate deposition, pozzolanic solution, sodium silicate, and carbonation were practised for strengthening the adhere mortar properties of TRCA [51–56]. These procedures to date challenge the economy, demand of skilled labour, durability, and adaptation flexibilities in real-time practices. In the present

Table 1 Chemical composition and physical properties of FFA, UCCNA, CCNA, and OPC

Properties				FFA	UCCNA	CCNA	OPC
Physical properties of FFA, UCCNA, CCNA, and OPC							
Specific gravity				2.81	2.89	3.11	3.14
Specific surface area (m^2/kg)				456	451	594	353
Fineness (%)				4.52	1.85	2.05	3.57
Oxide Composition (%)	FFA	UCCNA	CCNA	ASTM C618-19 Requirements [62]		OPC	ASTM C150/C150M – 20 Requirements for OPC [63]
				Pozzolana	Pozzolana + cementitious		
Chemical composition of FFA, UCCNA, CCNA, and OPC							
CaO	1.10	16	25.80	< 18%	> 18%	63.19	61–69
SiO_2	56.8	8.63	11.00	$SiO_2 + Al_2O_3 + Fe_2O_3$ = 50 to 70% min		21.18	18–24
Al_2O_3	30.23	12.56	13.31			6.18	2.6–8.0
Fe_2O_3	2.96	29.12	27.93			4.81	1.5–7.0
MgO	0.36	0.11	0.11			1.51	0.5–4.0
K_2O	1.38	8.45	10.16			0.63	0.2–1.0
Na_2O	0.11	2.16	2.956			0.13	-
SO_3	0.19	0.118	0.119	5% max		1.15	0.2–4.0
LOI	2.72	5.69	2.15	10% max		1.25	5.0 max

investigation, these challenges promote the adoption of novel freezing–thawing cyclic treatment to TRCA; this treatment aims to enhance the brittleness property of adhering mortar, which further assists for the easier removal when TRCA is subjected to external impact loading. The further study aims to develop a sustainable TRCA incorporated SCC mix through the BAGT method. The adaptation of BAGT aims to determine the best suitable replacement of TRCA in terms of both coarse and fine aggregates, which are based on the compliance requirements of compressive strength, flexural strength, and modulus of elasticity as per IS 456: 2000 [57]. Further, the performance of TRCA incorporated SCC was evaluated with CCNA and UCCNA.

Materials

Binder materials

Preliminary binder responsibility was taken care of by OPC with the density of 3140 kg/m^3, and mineral addition including class F-Fly-Ash (FFA) with the density of 2810 kg/m^3, UCCNA with 2890 kg/m^3, and CCNA with 3110 kg/m^3 was used as powder material in the SCC mixture. Detailed chemical composition and physical properties of FFA, UCCNA, CCNA, and OPC are presented in Table 1. The chemical composition reveals about pozzolanic nature of FFA, UCCNA, and CCNA as the summation of SiO_2, Al_2O_3, and Fe_2O_3 was found to be 89.99%, 50.31%, and 52.24%, respectively. In addition to this, CCNA even represents the cementitious properties because it has 25.80% of CaO. The physical appearance of binders was evaluated through Field Emission Scanning Electron Microscopy (FE-SEM) images on Carl Zeiss, Oxford equipment that assisted in understanding the particle morphology of binders. Figure 1 reveals the spherical structure of FFA and dense structure of OPC, CCNA, which have been taken with 5 kV acceleration voltages at a 2.8–4.5 mm working distance. CCNA represents the presence of voids due to the burnout of carbon during calcination [58]. UCCNA represents medium- to small-sized particles, which indicates the uncertainty of particle shape, size, and structure. In addition, the FE-SEM spectrum images have been confirming the presence of pozzolanic elements like Ca, Si, Al, O, and Fe concerning all binder variants. Figure 2 represents X-ray diffraction (XRD), particle size distribution, thermo-gravimetric analysis (TGA), and Fourier transform infrared spectroscopy (FTIR) analysis of binder materials. Figure 2a represents the mineralogical constituents of UCCNA and CCNA which includes portlandite ($Ca(OH)_2$), cristobalite (Si_4O_8), magnetite ($Fe_{24}O_{32}$), and gibbsite ($A_{l8}O_{24}$) as major compounds. Gehlenite ($Ca_4Al_4Si_2O_{14}$) and calcium silicate (Ca_2SiO_4) are found to be major mineralogical constituents of FFA and OPC. Detailed information regards compounds are presented in Table 2. Particle fraction details of binders are presented in Fig. 2b, which revealed that UCCNA was found to be coarser followed by OPC, CCNA, and FFA. The mean diameter (d_{50}) of CCNA and FFA was found to be 9 µm and followed by the mean diameter (d_{50}) of UCCNA and OPC to be 15 and 14 µm. Figure 2c represents the TGA performance

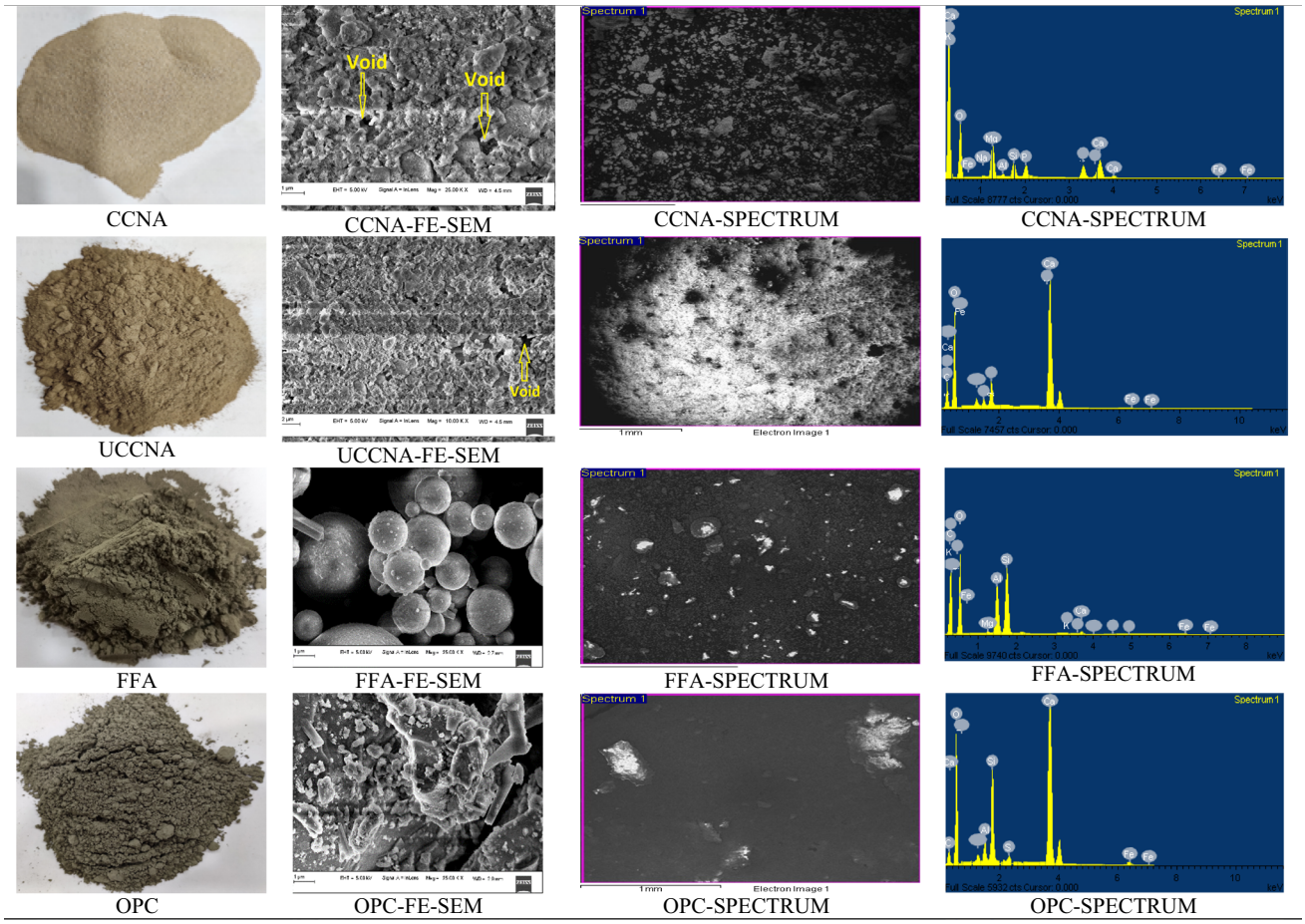

Fig. 1 FE-SEM and spectrum images of binders

of the binder, initial weight loss of binder between 36 and 230 °C was due to the presence of water [59], it was observed that loss of weight up to – 17.33% was found for UCCNA followed by – 2.43% for CCNA and – 0.19% for OPC and FFA. At the range of 280–510 °C, loss of weight was due to the escape of carbon [60]. Major weight loss of about – 5.56% was observed for UCCNA, followed by – 2.18% for CCNA, – 0.88% for OPC, and – 0.17% was found for FFA. Further at the range of 540–710 °C, major weight loss due to escape of left out unburnt carbon [58] of about – 7.68% was found for UCCNA followed by – 2.97% for OPC, – 1.12% for CCNA, and – 0.79% for FFA. Chemical bond details were examined by FTIR analysis as presented in Fig. 2d; OPC peaks between 2100 and 2300 cm^{-1}, 1400–1500 cm^{-1}, 1100–1200 cm^{-1}, 1011–1080 cm^{-1}, 877–878 cm^{-1}, 847–848 cm^{-1}, and 656–658 cm^{-1} wavenumbers may represent the presence of $CaCO_3$, CO_3, SO_4, polymerized silica, CO_3, Al–O or Al–OH, and SiO_4 [61]. In the context of pozzolanic material, peaks at 1098 cm^{-1}, 1072 cm^{-1}, and 1068 cm^{-1} of FFA, UCCNA, and CCNA may represent the presence of CO_3. In the fingerprint region of FTIR (600 cm^{-1} to 1400 cm^{-1}) comparison of CCNA and UCCNA more or less was found to be a closer impression. This may be due to the presence of similar chemical bonds. Overall microstructure assessment of binders about microtexture, compounds, particle fractions, combustion behaviour, and identified chemical bonds was in line with the oxide composition of binders.

Natural aggregates (NA)

For the preparation of control mix (CM) with 100% natural aggregate, 20 mm down locally available natural crushed coarse aggregates were utilized. River sand having a size less than 4.75 mm was utilized as fine aggregate. In addition to SCC mixes, the emphasis was switched away from natural aggregates and towards TRCA replacement.

Total recycled concrete aggregates (TRCA)

TRCA was extracted from concrete laboratory waste. Further bifurcation of these aggregate was carried through a drilling

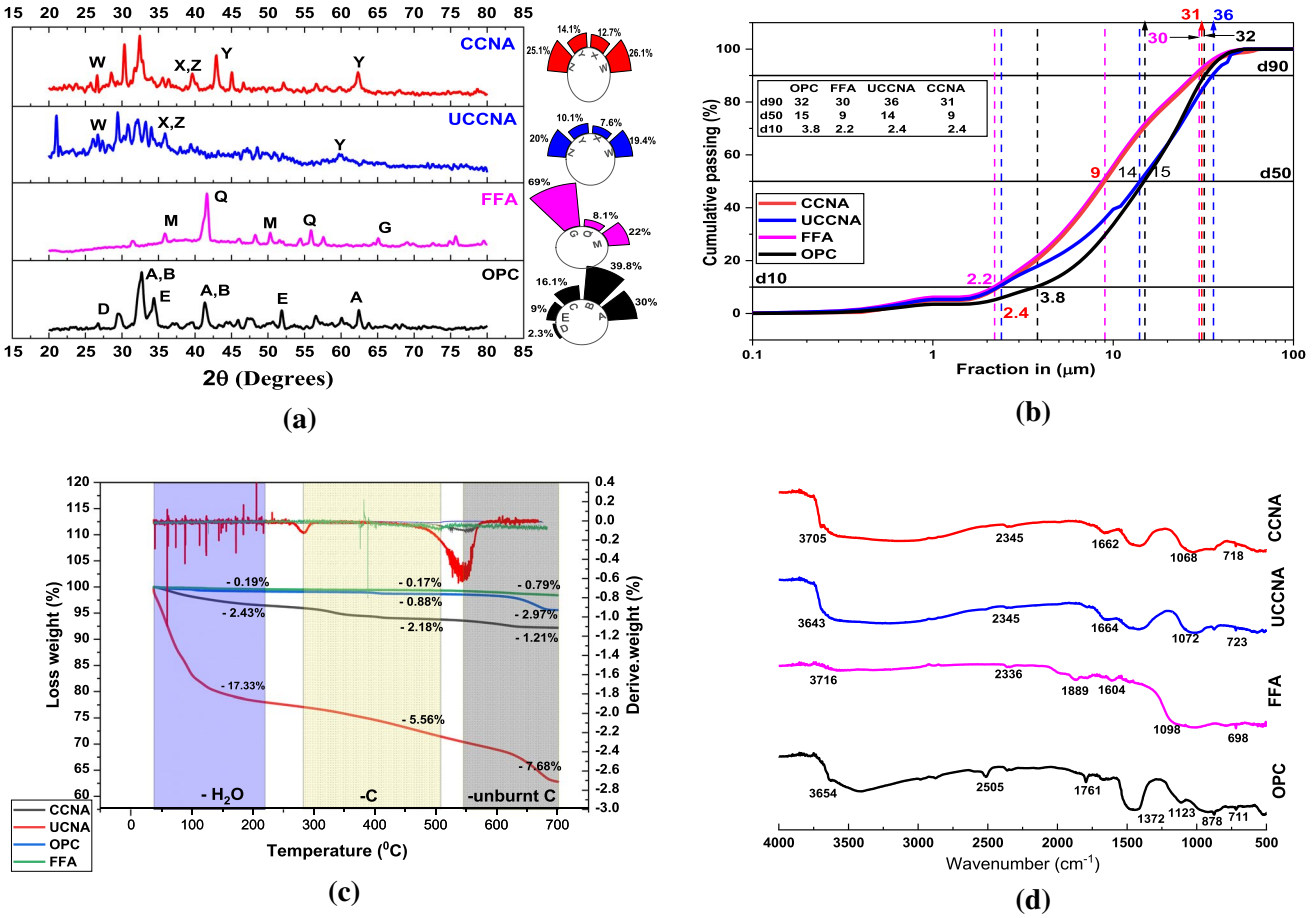

Fig. 2 XRD (**a**), particle size distribution (**b**), TGA (**c**), and FTIR (**d**) of binder materials

Table 2 Identification for the compound name and chemical formula of binder materials

UCCNA and CCNA			
W	96-900-6835	Portlandite	$Ca(OH)_2$
X	96-901-5088	Cristobalite	Si_4O_8
Y	96-900-5839	Magnetite	$Fe_{24}O_{32}$
Z	96-901-5977	Gibbsite	$A_{l8}O_{24}$
FFA			
M	96-901-0160	Mullite	$Al_{4.56}Si_{1.44}O_{9.72}$
Q	96-710-3015	Quartz	Si_3O_6
G	96-101-1003	Gehlenite	$Ca_4Al_4Si_2O_{14}$
OPC			
A	01-070-1846	Calcium silicate oxide	$Ca_3(SiO_4)O$
B	00-029-0371	Calcium silicate	Ca_2SiO_4
C	01-070-0134	Calcium aluminium oxide	$CaA_{l2}O_4$
D	01-074-0803	Iron aluminium calcium oxide	$Fe_2O_3A_{l2}O_3(CaO)_4$
E	01-072-0596	Calcium sulphate hydrate	$Ca\ (SO_4)(H_2O)_2$

machine as presented in Fig. 3a. As in Fig. 3b refining of destressed TRCA was carried through the aggregate grinding machine; further, TRCA coarse aggregates (≥4.75 mm) and TRCA fines (≤4.75 mm) were collected and stored separately. Further treatment to TRCA fractions was necessary to remove the adhering mortar because the previous investigation revealed that the presence of adhering mortar significantly reduces the concrete characteristics [41, 64, 65]. In addition, SCC rheological performance was significantly reduced while utilizing untreated TRCA as a major source of an aggregate fraction [66–68]. To encounter these uncertainties, ageing protocols for TRCA fractions were purposefully carried out. In this, TRCA aggregate underwent freezing and thawing cyclic procedure, which imparts brittle property in adhering mortar of TRCA. It is necessary for easy removal of adhering mortar while experiencing the impact loading in the ABAT chamber. Further, these aggregate fractions were sieved (Fig. 4) and stored separately.

Chemical admixture

For the promotion of rheological properties of a concrete mixture, a superplasticizer (SP) based on modified

(a) (b)

Fig. 3 Bulk TRCA distressing from concrete waste (**a**) refining the distressing material through the aggregate grinding machine (**b**)

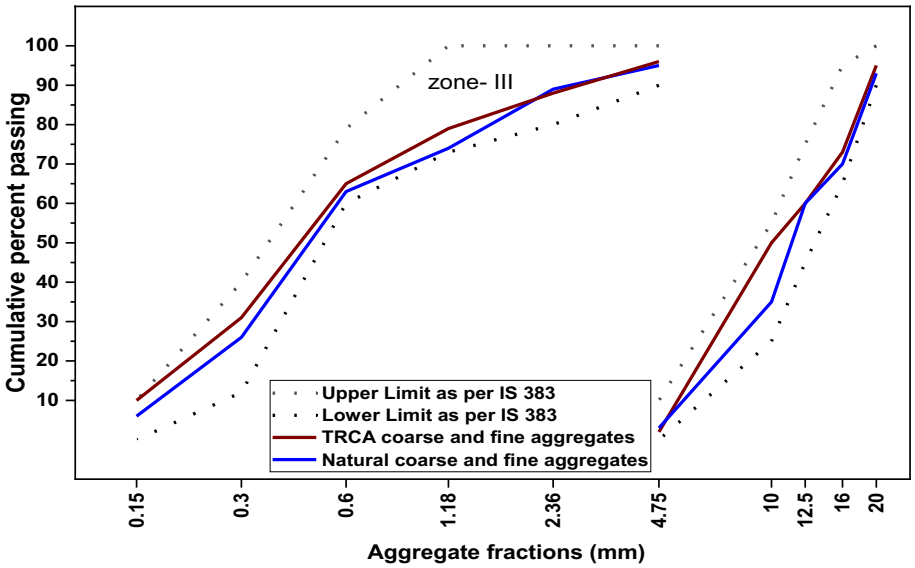

Fig. 4 Natural and TRCA aggregate fractions

polycarboxylic ether polymer with a specific weight of 1.085 kg/litre and pH of 6 was used. The manufacturer recommended a dosage range of 0.5–3.0 L/1000 kg of cementitious materials.

Methodology

CCNA preparation process

CCNA made from cashew nut shells was sun-dried for 14 days before being calcined in a gas furnace chamber at 750 °C for 8 h. It was also sieved through 45 m for fraction separation to match the particle size of OPC.

TRCA optimization with novel freeze and thaw cyclic treatment

Initially, fractioned TRCA is underwent heat treatment. TRCA was kept in an oven by maintaining the temperature of about 250 °C for about 24 h. Further TRCA was cooled down to room temperature and adhere mortar removing process was executed in the ABAT chamber. As in Fig. 5, it was found that 10 CB would be optimal because further increment of CB was found to be insignificant towards the removal of adhering mortar from TRCA, which results in no change in water absorption (WA). For the further removal of adhered mortar, these TRCA aggregates undergo freezing and thawing (F&T) cycles. In this, TRCA was sealed in plastic bags and kept in a freezer at – 18 °C for 24 h. Further unwrapped TRCA was carted out and kept in the container with water immersion at 80 °C for 24 h, which implies one cycle completion. This experiment reveals seven cycles as optimal, and adaptation of twelve cycles was found to be

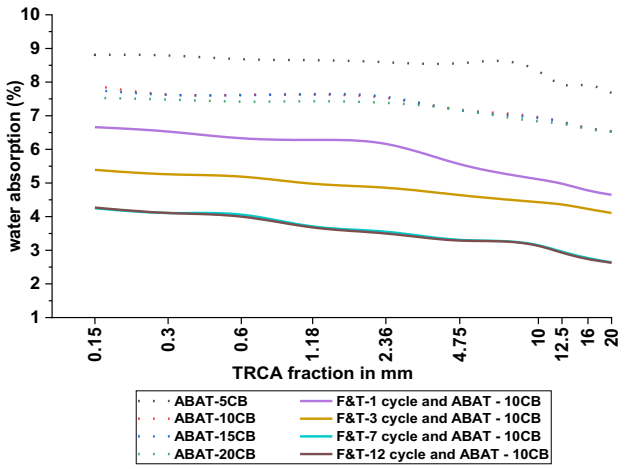

Fig. 5 Water absorption versus TRCA fraction

insignificant regards the removal of adhering mortar from TRCA. Figure 6 is the representation of the physical characteristics transition of TRCA throughout the treatment process. As per previous studies and IS 383 [69] aggregate particles were restricted to 150 µm or more, and particles less than 150 µm were considered as binder particles or fillers. This promotes the rejection of fine TRCA of about 75 µm or less from the present investigation. Further, treated TRCA were fractioned through sieves and stored as Coarse TRCA (C-TRCA) and Fine TRCA (F-TRCA). Figure 7 demonstrates the final appearance of each TRCA fraction, and it was found that on average, 2.94% and 3.91% WA characteristics remained in treated C-TRCA and F-TRCA fractions, respectively.

Fig. 6 Change of TRCA aggregates physical characteristics during the treatment process

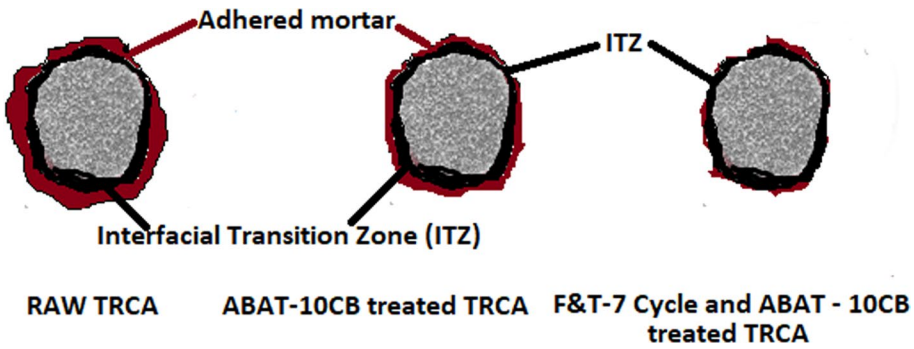

Fig. 7 F&T–7 cycle and ABAT–10CB treated TRCA

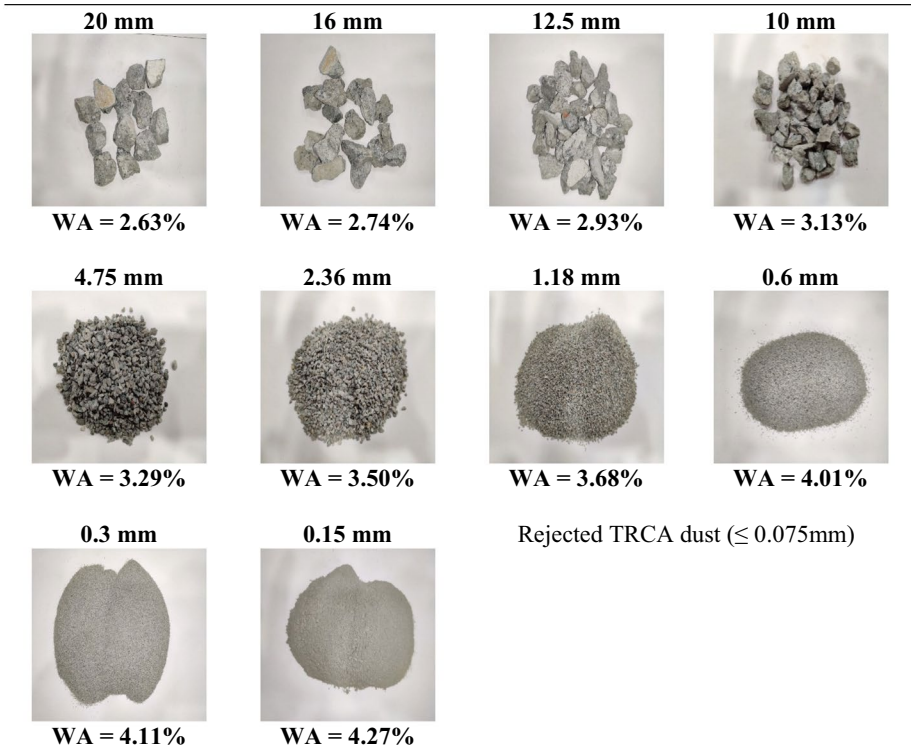

Gradation optimization utilizing the Bailey aggregate grading technique

Bailey's aggregate grading technique (BAGT) allows the gradation selection based on nominal maximum aggregate size (NMAS = 20 mm) and particle orientation factor (POF). Characterization of NA and TRCA aggregate is as in Table 3. In SCC, it was expected that concrete must gain the flowing, filling, and passing ability, which primarily relies on mortar and aggregate orient fraction. In the context of aggregate orient fraction, BAGT was the most suitable technique regards gradation selection for SCC. POF was measured based on loose unit weight (LUW) and rodded unit weight (RUW) of aggregate characteristics. LUW was a representative of POF of aggregate without external effort, and RUW was a representative of POF of aggregate at three-layer compacted state. BAGT prefers the selection of gradation based on the self-orientation of aggregate particles without external effort through the blending process, which results in the selection of chosen unit weight (CUW). CUW is always lying around LUW and RUW. As per BAGT, CUW must fall in between 95 and 105% of LUW. In the present design, CUW was considered equivalent to LUW or CUW = 100% of LUW. The reason behind these considerations was to eliminate the gradation packing error, which might occur in SCC as further selected gradation must compensate with cement mortar with the least ± 5% variance of LUW. Further, BAGT relays on NMAS, POF, and voids of coarse and fine aggregates. Usually in BAGT, gradation relays on control sieves which were Half Sieve (HS = NMAS/2), Primary Control Sieve (PCS = NMAS*0.23), Secondary Control Sieve (SCS = PCS*0.23), and Tertiary Control Sieve (TCS = NMAS*0.23). A two-dimensional (2D) and three-dimensional (3D) analysis of the packing of different fractions yielded the estimated value of 0.23. According to previous studies, the average particle diameter ratio ranges from 0.15 (for round and hexagonal close-packed particles) to 0.42 (consideration of flat and cubical packed particles) [32, 34, 36, 37]. Exploration of particle packing revealed that particle packing follows various models, with the trademark measurement being above or below 0.23 proportions, so 0.23 was considered to be the normal state of packing design [32, 37]. In the present study, 20 mm was NMAS, 10 mm was HS, 4.75 mm was PCS, 1.18 mm was SCS, and 0.3 mm was TCS. In addition, POF and gradation boundary conditions were evaluated and controlled through coarse aggregate ratio (Ca-ratio) (Eq. 1), fine aggregate coarser ratio (Fac-ratio) (Eq. 2), and fine aggregate finer ratio (Faf-ratio) (Eq. 3) which were collectively called Bailey ratios.

$$\text{Ca-ratio} = \frac{(\%\text{Passing HS} - \%\text{Passing PCS})}{(100\% - \%\text{Passing HS})} \tag{1}$$

$$\text{Fac-ratio} = \frac{\%\text{Passing SCS}}{\%\text{Passing PCS}} \tag{2}$$

$$\text{Faf-ratio} = \frac{\%\text{Passing PCS}}{\%\text{Passing TCS}} \tag{3}$$

BAGT recommended Bailey ratio ranges from 0.6 to 0.75 for Ca-ratio and 0.35 to 0.5 for Fac-ratio and Faf-ratio. Bailey ratios must be between recommended ranges after gradation design to ensure better particle orientation, interaction, and packing.

Mix design as per compliance requirement of SCC

The present study aims to develop a sustainable SCC mix of M40 grades. Cement being a primary binder contributes 75% and FFA being a secondary binder contributes

Table 3 Characterization of NA and TRCA aggregate

	NA		TRCA			
	CA	FA	CA	FA		
Control Sieve			PCS	SCS	TCS	TCSP
Control Sieve sizes (mm)	≤ 20 to ≥ 4.75	≤ 4.75 to ≥ 1.18	≤ 20 to ≥ 4.75	≤ 4.75 to ≥ 1.18	≤ 1.18 to ≥ 0.3	≤ 0.3
LUW (kg/m^3)	1394	1348	1386	1358	1348	1342
				TRCA-FA = 1347		
RUW (kg/m^3)	1540	1353	1536	1373	1396	1392
				TRCA-FA = 1391		
Change in unit weight (%)	10.47	0.37	10.82	1.04	3.56	3.73
				TRCA-FA = 3.26		
WA (%)	1.56	2.18	3.94	4.61	5.01	5.28
Specific Gravity	2.60	2.54	2.56	2.53	2.43	2.41

TCSP—tertiary control sieve passing means—are the fractions retained in 150μ sieve

Optimum mixes (OM) are in bold

25% in the control mix (CM) of SCC. CM was prepared with 100% natural aggregate with a 0.34 water to powder ratio. As per IS 456, [57] target strength of CM aims towards gaining about 48.25 Mpa at the age of 28 days. Further C-TRCA was introduced in the SCC at a 25% incremental rate up to 100% with the BAGT technique. Identification of possible maximum replacement (MR) was evaluated as per clauses 16.1 and 16.3 of IS 456 [57]. For M40 graded concrete compliance, the requirement of compressive strength (f_{cr}) was 44.13 MPa as found by Eq. (4). For identifying compliance, requirements of flexural strength (f_{fx}) and modulus of elasticity standard recommended prediction equations were utilized as per IS 456 [57] norms. It was found to be 4.65 MPa and 33.22 GPa regards flexural strength (f_{fx}) and modulus of elasticity (M_{el}) as in Eqs. (5) and (6) [57]. Once after the identification of possible maximum replacement percentage of C-TRCA, it was decided to be kept constant for further additional all SCC mixes.

$$f_{cr} = f_{ckt} + (0.825 \times \sigma t) \text{ or } f_{ckt} + 4 \text{(either is greater)} \quad (4)$$

$$f_{fx} = 0.70\sqrt{f_{cr}} \quad (5)$$

$$M_{el} = 5\sqrt{f_{cr}} \quad (6)$$

where

f_{ckt} is characteristic strength of concrete and it is 40 MPa for M40 grade.

σt is the standard deviation and it is found to be 5 for M40 grade concrete as per IS 456 [57].

In addition to SCC mixes, C-TRCA percentage (based on MR) was kept constant and F-TRCA was introduced at a 25% incremental range up to 100% replacement. The possible maximum replacement percentage of F-TRCA was further determined based on the compliance requirements of SCC. Further, it was decided to keep these identified MR percentages of C-TRCA and F-TRCA constant in supplementary SCC mixes. As observed from Table 3, the change in unit weight percentage of coarse NA (10.47%) and C-TRCA (10.82%) was found to be similar. However, the difference in change in unit weight percentage between fine NA (0.37%) and F-TRCA (3.26%) was found to be 2.89%. It revealed poor particle orientation and poor compacting abilities of F-TRCA. The presence of more adhered mortar in F-TRCA would be the reason for poor performance. Further, it was necessary to perform optimization by altering the incorporated percentage of F-TRCA and it was carried out. As detailed in Table 4, the incorporated percentage of F-TRCA was altered between 75 and 95% in SCS with an incremental trend. At the same time, F-TRCA introducing percentages in TCS and TCSP were reduced from 75 to 65% at a decremental trend. As a finalized result, an optimized SCC mix was chosen based on compliance requirements of rheological and mechanical properties. Extended SCC mixes were performed with the aim of paste optimization by replacing cement with UCCNA and CCNA at a 5% replacement rate up to 20%.

Fresh state and solid-state test methods of SCC

Fresh state properties of SCC were examined by slump flow test, T_{500} slump flow test, and V-funnel test as per EFNARC guidelines [70]. Solid-state properties of SCC were examined by compression strength test, split tensile strength test, flexural strength test, and modulus of elasticity test at the age of 7, 28, and 90 days as per IS 516 [71, 72]. 150 mm × 150 mm × 150 mm cube-sized mould was utilized to cast compression test samples, followed by 100 mm × 100 mm × 500 mm mould utilized for flexural test samples, and 150 mm × 300 mm cylinders moulds were utilized for split tensile and modulus of elasticity test samples [71–73].

Microstructure evaluation of SCC binders

Microstructure evaluation was carried out for paste combinations. Field Emission Scanning Electron Microscope (FE-SEM) test by employing Carl Zeiss FE-SEM, Oxford instrument was performed on OPC, followed by binary and ternary binder combinations. Mineralogical compounds and chemical formulas of chemical constituents were examined by XRD spectroscopic analysis, and it was performed using a Rigaku Mini-flex with an angle measurement of (5°–130°) 2θ value. Energy-dispersive spectroscopy (EDS) was performed on binary and ternary binder combinations to investigate and measure the chemical elements of binder residues. TGA procedure was utilized to determine the thermal characteristics of binary and ternary binder combinations. TGA was accomplished in the selection of 30–790 °C at the rate of 10 °C/minute utilizing the discovery series TA-55 instrument. FTIR utilizing JASCO FT/IR-6300 with a wavelength range of 400–4000 cm^{-1} was performed on binary and ternary paste combinations. In the context of microstructure evaluations, regard, all binders were performed respective tests at the age of 7 (early stage of curing) and 90 (later stage of curing period) days.

Table 4 SCC mix design TRCA

Concrete Mixes	Ca-ratio (0.6–0.75)	Fac-ratio (0.35–0.50)	Faf-ratio (0.35–0.50)	Retained (kg/m^3)			Passed (kg/m^3)					
				PCS (≥4.75 mm)	SCS (≥1.18 mm)	TCS (≥0.3 mm)	TCSP (≤0.3 mm)	FA/CA	OPC (kg/m^3)	FFA (kg/m^3)	CCNA or UCCNA (kg/m^3)	SP (kg/m^3)
				NA + TRCA	NA + TRCA	NA + TRCA	NA + TRCA					
CM	0.75	0.48	0.50	770 + 0	378 + 0	176 + 0	176 + 0	0.95	450	150	NA	0.925
TRCA-CA25	0.74	0.48	0.50	575 + 191	383 + 0	175 + 0	175 + 0	0.96	450	150	NA	1.715
TRCA-CA50	0.72	0.47	0.50	380 + 380	388 + 0	174 + 0	174 + 0	0.97	450	150	NA	1.735
TRCA-CA75	**0.71**	**0.47**	**0.50**	**189 + 567**	**395 + 0**	**174 + 0**	**174 + 0**	**0.98**	**450**	**150**	**NA**	**1.755**
TRCA-CA100	0.70	0.47	0.50	0 + 752	399 + 0	174 + 0	174 + 0	0.99	450	150	NA	1.790
TRCA-CA75-FA25	0.70	0.47	0.50	188 + 563	295 + 98	134 + 45	134 + 45	0.99	450	150	NA	1.800
TRCA-CA75-FA50	0.68	0.48	0.50	186 + 558	196 + 196	91 + 91	90 + 90	0.97	450	150	NA	1.835
TRCA-CA75-FA75	**0.67**	**0.49**	**0.49**	**184 + 553**	**97 + 293**	**47 + 140**	**46 + 141**	**0.96**	**450**	**150**	**NA**	**1.865**
TRCA-CA75-FA100	0.66	0.49	0.49	183 + 549	0 + 391	0 + 191	0 + 190	0.95	450	150	NA	1.880
TRCA-CA75-FA75-1	0.68	0.45	0.43	185 + 556	62 + 351	60 + 138	44 + 103	1.02	450	150	NA	1.860
TRCA-CA75-FA75-2	**0.69**	**0.45**	**0.35**	**186 + 559**	**22 + 412**	**73 + 135**	**40 + 73**	**1.01**	**450**	**150**	**NA**	**1.860**
TRCA-CA75-FA75-2-CCNA5	0.69	0.45	0.35	186 + 559	22 + 412	73 + 135	40 + 73	1.01	427.50	150	22.5	1.935
TRCA-CA75-FA75-2-CCNA10	0.69	0.45	0.35	186 + 559	22 + 412	73 + 135	40 + 73	1.01	405	150	45	1.960
TRCA-CA75-FA75-2-CCNA15	**0.69**	**0.45**	**0.35**	**186 + 559**	**22 + 412**	**73 + 135**	**40 + 73**	**1.01**	**382.50**	**150**	**67.5**	**1.985**
TRCA-CA75-FA75-2-CCNA20	0.69	0.45	0.35	186 + 559	22 + 412	73 + 135	40 + 73	1.01	360	150	90	2.000
TRCA-CA75-FA75-2-UCCNA5	**0.69**	**0.45**	**0.35**	**186 + 559**	**22 + 412**	**73 + 135**	**40 + 73**	**1.01**	**427.50**	**150**	**22.5**	**1.935**
TRCA-CA75-FA75-2-UCCNA10	0.69	0.45	0.35	186 + 559	22 + 412	73 + 135	40 + 73	1.01	405	150	45	1.960

Table 4 (continued)

Concrete Mixes	Ca-ratio (0.6–0.75)	Fac-ratio (0.35–0.50)	Faf-ratio (0.35–0.50)	Retained (kg/m^3)			Passed (kg/m^3)				
				PCS (≥4.75 mm)	SCS (≥1.18 mm)	TCS (≥0.3 mm)	TCSP (≤0.3 mm)	FA/CA	OPC (kg/m^3)	FFA (kg/m^3)	CCNA or UCCNA (kg/m^3)	SP (kg/m^3)
				NA + TRCA	NA + TRCA	NA + TRCA	NA + TRCA					
TRCA-CA75-FA75-2-UCCNA15	0.69	0.45	0.35	186 + 559	22 + 412	73 + 135	40 + 73	1.01	382.50	150	67.5	1.985
TRCA-CA75-FA75-2-UCCNA20	0.69	0.45	0.35	186 + 559	22 + 412	73 + 135	40 + 73	1.01	360	150	90	2.000

TRCA-CA75-FA75—(75% TRCA in PCS + 75% TRCA in SCS + 75% TRCA in TCS + 75% TRCA in TCSP); TRCA-CA75-FA75-1—(75% TRCA in PCS + 85% TRCA in SCS + 70% TRCA in TCS + 70% TRCA in TCSP); TRCA-CA75-FA75-2—(75% TRCA in PCS + 95% TRCA in SCS + 65% TRCA in TCS + 65% TRCA in TCSP)—here Faf-ratio reaches the minimum limit

Optimum mixes (OM) are in bold

Quality assessment of SCC

Quality of SCC was evaluated at the age of 28 days utilizing the ultrasonic pulse velocity (UPV) test as per IS 13311 (Part 1) [74]. As per standards, UPV values varying between less than 3000 m/s, 3000 m/s to 3500 m/s, 3500 m/s to 4500 m/s, and more than 4500 m/s concrete quality were evaluated as weak, modest, adequate, and excellent. In addition, drying shrinkage, WA, and density parameters of SCC were also evaluated to recognize the qualified performance of concrete along the same lines (Fig. 8).

Results and discussion

Fresh state properties of SCC

Fresh state properties of SCC were evaluated based on the flowing ability and viscosity class. The increase of C-TRCA and F-TRCA reduces the flowing ability of SCC, which results in higher viscosity. As the percentage contribution of TRCA increases, WA in the overall mix increases, which was the preliminary reason for the drop of slump flow, slump $T_{500,}$ and V-funnel performances [75–77]. However, poor particle orientation characteristics of TRCA (change in unit weight percentage of F-TRCA is 3.26% as in Table 3) was the secondary reason for the reduction of fresh state characteristics of SCC. In addition, the preparation process of TRCA produces more irregularity regards aggregate shape, texture, which makes it difficult to flow in a blended paste [66, 78, 79]. All SCC mixes successively achieved the minimum fresh-state requirements, which included slump T_{500} (≥ 2 s), V-funnel (≥ 8 s), and slump flow (≥ 550 mm) except TRCA-CA75-FA100. This classifies the SCC as SF-1 and VS1/VF1 class as per EFNARC standards [70]. Relative slump flow, slump T_{500}, and V-funnel revealed about decrease of 4.09% slump, an increase of 4.25% slump T_{500}, and an increase of 4.31% V-funnel performances, which declares the failure of TRCA-CA75-FA100 SCC. Slump flow, slump $T_{500,}$ and V-funnel performance of TRCA-CA100 and TRCA-CA75-FA50 appeared to be identical. It may be due to the achievement of similar compensative WA characteristics of both TRCA-CA100 and TRCA-CA75-FA50 mixes. However, superplasticizer demands for TRCA-CA75-FA50 (1.835 kg/m^3) were found to be more than TRCA-CA100 (1.790 kg/m^3) due to the increased surface area of F-TRCA. TRCA-CA75-FA75-1 and TRCA-CA75-FA75-2 have optimized SCC mixes; reduction of F-TRCA in TCS and TCSP (75% to 65%) by contributing compensated F-TRCA in PCS (75% to 95%) reduces the WA demand in the overall SCC mix by enhancing the fresh state properties. It revealed that restriction of F-TRCA (≥ 1.18 mm) in

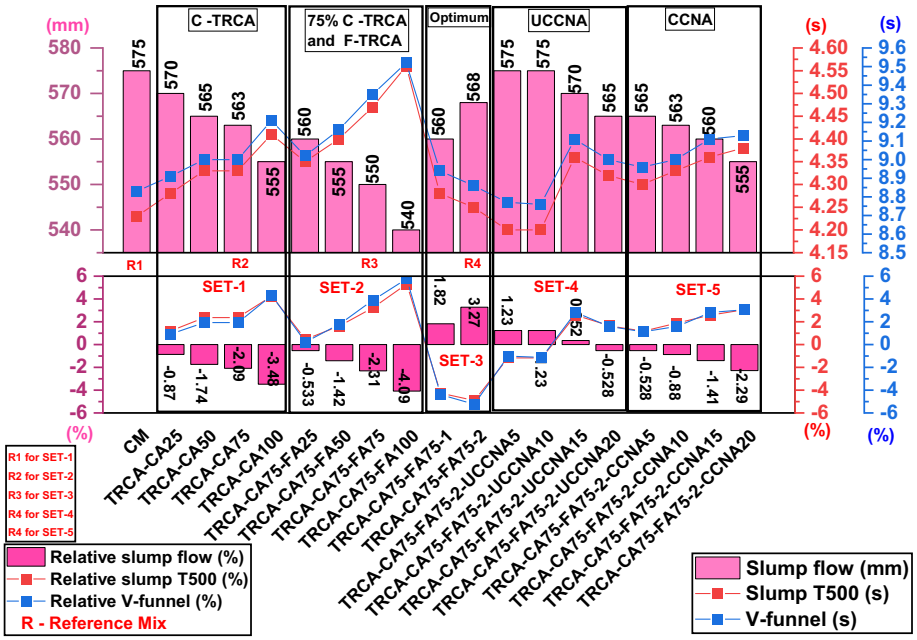

Fig. 8 Fresh-state properties of SCC

TRCA-CA75-FA75-2 enhances relative performances of slump flow, slump $T_{500,}$ and V-funnel by 3.27%, − 4.92%, and − 5.24%, respectively. Overall TRCA-CA75-FA75-2 was the optimized TRCA-based SCC mix, which sustained the identical performance of TRCA-CA25 with a higher superplasticizer demand of about 1.860 kg/m^3.

Further performance of TRCA-CA75-FA75-2 was analyzed in the presence of UCCNA. In the presence of UCCNA, 5% (TRCA-CA75-FA75-2-UCCNA5) relative slump flow was increased by 1.23% and even the same performance was sustained at 10% UCCNA (TRCA-CA75-FA75-2-UCCNA10) replacement. Synchronously slump T_{500} and V-funnel relative performance were reduced by − 1.17% and − 1.02% at 5% to 10% UCCNA replacement levels. The presence of more unburnt carbon (confirmed by TGA analysis as in Fig. 2c) retards the initial state of hydration when gets contacted with water, and UCCNA was much finer than OPC (confirmed by particle size distribution analysis as in Fig. 2b); its d_{50} (14 µm) and d_{10} (2.4 µm) were finer than that of OPC d_{50} (15 µm) and d_{10} (3.8 µm), which resulted in improved fresh-state performances of SCC up to 10% UCCNA level. At further replacement level (TRCA-CA75-FA75-2-UCCNA15 and TRCA-CA75-FA75-2-UCCNA20) decremental trends regard of fresh state performances of SCC has appeared. The presence of uncertain UCCNA particle distribution (UCCNA d_{90} (36) > OPC d_{90} (32) as in Fig. 2b) may retard the fresh state properties of SCC at higher replacement levels of about 15% and 20%.

In addition, TRCA-CA75-FA75-2 was analyzed in the presence of CCNA. It was evident that as the increase of CCNA partial replacement percentage was by 5–20%, a reduction in fresh state properties was found. Usually, calcined agro-waste has a higher rate of reaction phase [2, 5], specifically with the presence of higher CaO (25.80%) and Fe_2O_3 (27.93%) in CCNA, which accelerates the initial hydration process [15]; in addition, CCNA (d_{50} = 9) was much finer than OPC (d_{50} = 15) which categorizes CCNA as higher reactive phase material, which results in the reduction of fresh state properties. As per relative slump flow, relative slump $T_{500,}$ and relative V-funnel, maximum performance drops were found for TRCA-CA75-FA75-2-CCNA20 by − 2.29%, + 3.05%, and + 3.04%, respectively.

Compressive strength of SCC

Compressive strength will be the core representation method regards to all types of concrete. In comparison with CM, it was found that as the replacement percentage of TRCA increases, decremental compressive strength was found. As per the compliance requirement of concrete, it was found that 75% (TRCA-CA75 and TRCA-CA75-FA75) will be the possible MR percentage regards to both the coarse and fines of TRCA through BAGT. Further replacement failed to fulfil the minimal compliance requirements of concrete. The presence of adhered mortar was the culprit that weakened the interfacial transition zone (ITZ) and became responsible for earlier failure of bonding between the packed aggregate regards TRCA-based SCC [80, 81]. In addition, relative compressive strength revealed maximum differentiation, specifically in SET-2 at the age of 7 days as in Fig. 9. Maximum decremental relative compressive strength was observed for TRCA-CA75-FA75 and TRCA-CA75-FA100 at the age of 7 days, and it was about − 15.42% and − 19.87%.

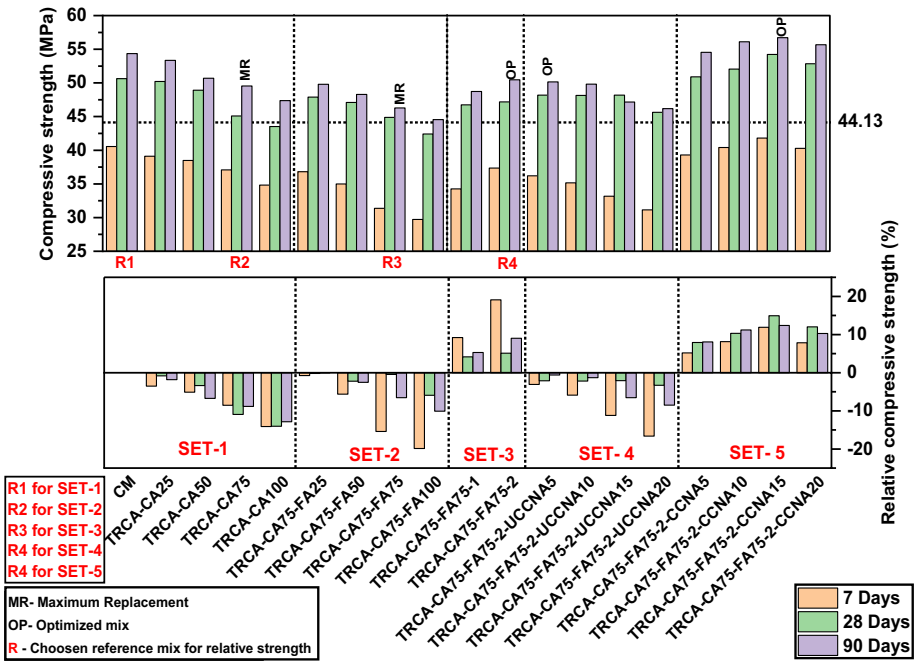

Fig. 9 Compressive strength of SCC

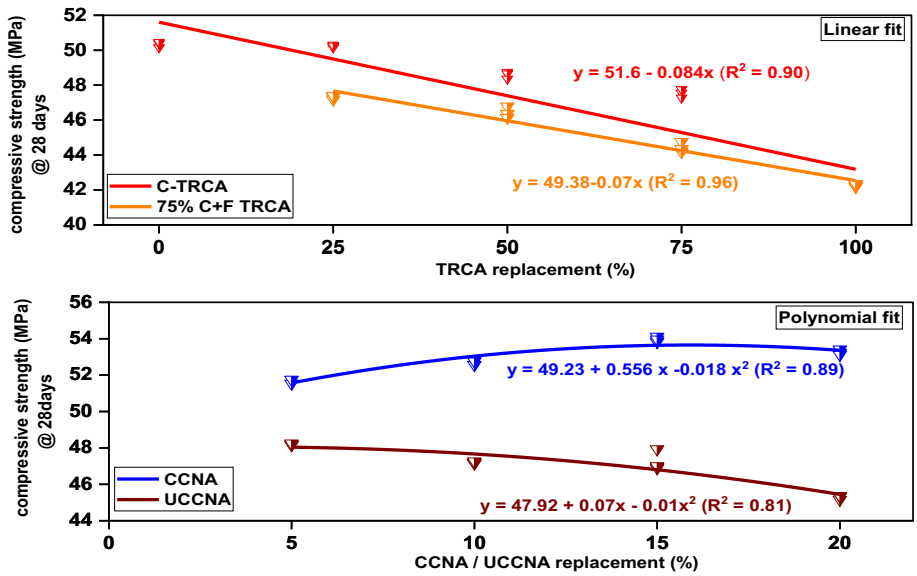

Fig. 10 Regression fit for compressive strength of SCC

It was evident that the presence of adhering mortar retards the earlier stage of hydration, which weakens the ITZ. Further gradation optimization through BAGT was carried out by minimizing F-TRCA in TCS and TCSP and by the same percentage of F-TRCA introduced in SCS, which improvised the compressive strength. Specifically for TRCA-CA75-FA75-2, incremental relative compressive strength was found at about + 19.11% at the age of 7 days. It was evident that a restriction of 1.18 mm or less sized F-TRCA aggregate through BAGT significantly promoted earlier age of compressive strength in TRCA-based SCC. Overall, as in Fig. 10, TRCA replacement was found to be significant concerning to compressive strength of TRCA-based SCC with 0.90 and 0.96 R^2 values.

The introduction of the prioritized UCCNA binder to TRCA-CA75-FA75-2 imparts negative performance. Exclusively, TRCA-CA75-FA75-2-UCCNA20 gained − 16.62% relative compressive strength. It was evident that the presence of more unburnt carbon (as in Fig. 2c), retards the hydration and imparts weaker ITZ structure in and around the TRCA, which results in poor performance. However, as per the compliance requirement of concrete, all UCCNA-based SCC mixes successfully fulfilled the minimal requirement. In addition, TRCA-CA75-FA75-2-UCCNA5 and

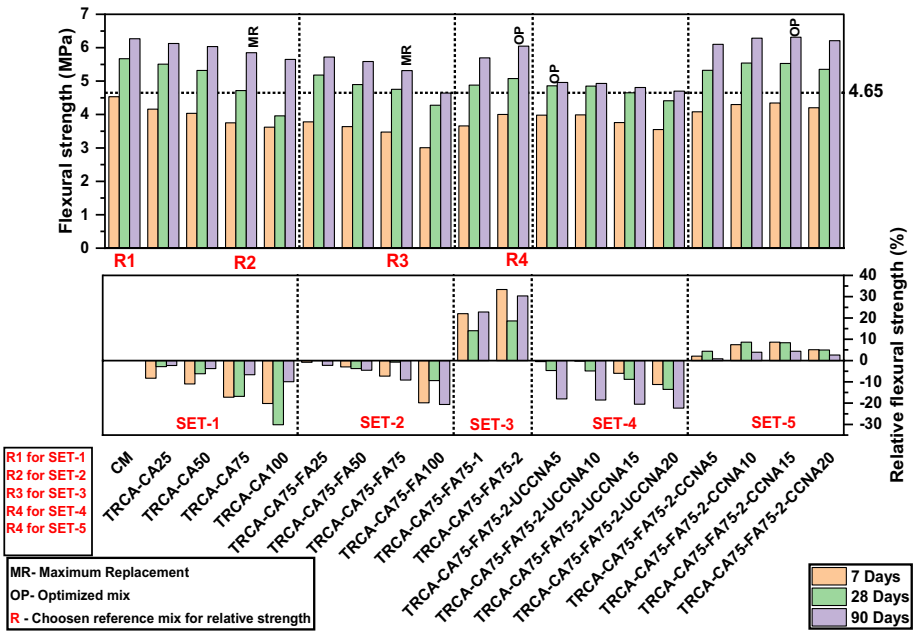

Fig. 11 Flexural strength of SCC

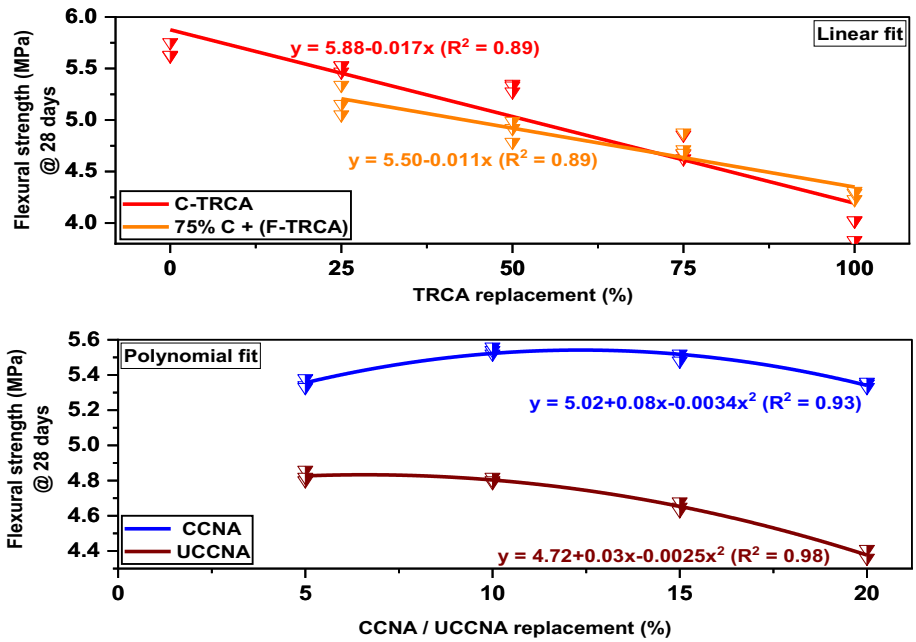

Fig. 12 Regression fit for flexural strength of SCC

TRCA-CA75-FA75-2-UCCNA10 were found to be optimal mixes.

Further introduction of prioritized CCNA binder to TRCA-CA75-FA75-2 imparts inventiveness regards compressive strength of SCC. As stated in Sect. 4.1, the presence of CaO (25.80%) and Fe_2O_3 (27.93%) in CCNA, accelerated hydration. Furthermore, CCNA ($d_{50}=9$) was much finer than OPC ($d_{50}=15$), classifying CCNA as a higher reactive phase material, resulting in ITZ as a dense composite structure. TRCA-CA75-FA75-2-CCNA15 was found to be an optimized SCC mix with + 14.94% of relative compressive strength. In addition, the relation between compressive strength versus UCCNA or CCNA replacement percentage was examined with a polynomial fit and it was found to be significant with 0.81 and 0.89 R^2 values.

Flexural strength of SCC

Performance evaluation of flexural strength revealed the same trend as of compressive strength characteristics of TRCA-based SCC. It was found that TRCA-CA100, TRCA-CA75-FA100, and TRCA-CA75-FA75-2-UCCNA20

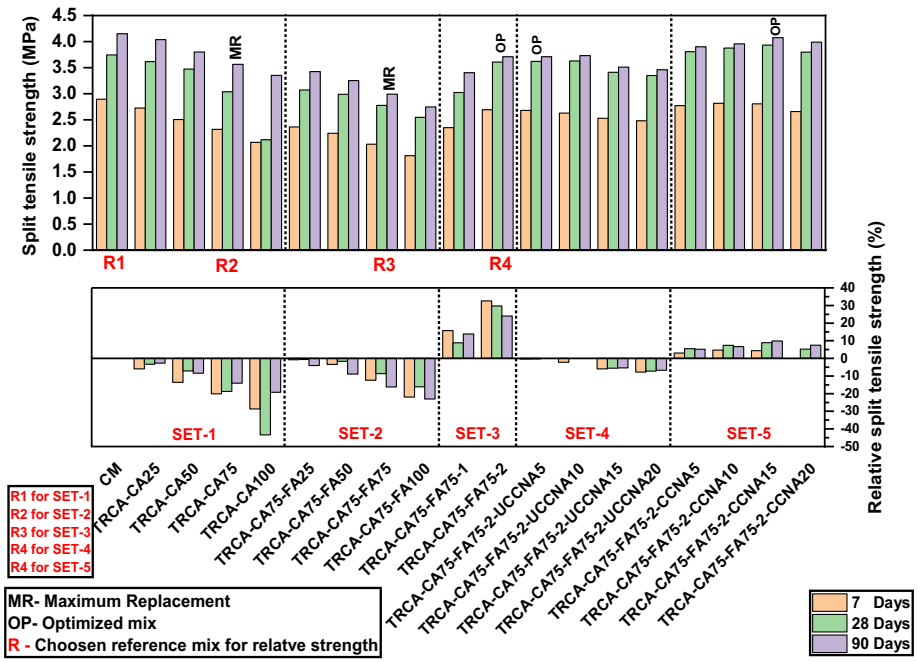

Fig. 13 Split tensile strength of SCC

were failed to fulfil the minimal compliance requirement of SCC and left-out SCC mixes were succeeded to fulfil the same as in Fig. 11. With the increase of TRCA, the WA rate of SCC also enhances. It exhibits more water demand required for the hydration process, which may result in poor construction of ITZ [82–84]. In addition, the presence of adhering mortar weakens aggregate interlocking characteristics (Refer Table 3), which results in poor flexural properties of TRCA-based SCC. The relative performance of TRCA-CA75-FA75-1 and TRCA-CA75-FA75-2 represents an increase of 22% and 33.33% at the age of 7 days, respectively.

It comes with the agreement that a reduction of 1.18 mm or less with the implication of BAGT enhanced the packing characteristics, which resulted in significant improvements of earlier strength of TRCA-based SCC. In addition, the relation between TRCA replacement percent versus flexural strength (Fig. 12) was found to be significant with a 0.89 R^2 value.

Performance of TRCA-CA75-FA75-2 with UCCNA blended binder was found to be failed regards improvement of relative flexural strength. Flexural performance of TRCA-CA75-FA75-2-UCCNA5 and TRCA-CA75-FA75-2-UCCNA10 was found to be similar in regard to 7, 28, and 90 days. As stated in Sect. 4.2, UCCNA has more unburnt carbon, which resulted in poor performance.

CCNA blended binder with TRCA improved the flexural performance of concrete, and it was found that TRCA-CA75-FA75-2-CCNA15 can be optimal. Relation revealed that the implication of UCCNA ($R^2 = 0.98$) and CCNA ($R^2 = 0.93$) has a significant influence over flexural characteristics of TRCA-based SCC.

Split tensile strength of SCC

Split tensile strength of concrete is in agreement with compression and flexural performance. As the replacement percentage of TRCA increases, a decremental trend was observed regards the tensile properties of concrete as in Fig. 13. Specifically, the implication of BAGT was found to be advantageous.

TRCA-CA75-FA75-1 and TRCA-CA75-FA75-2 succeeded in representing incremented relative split tensile strength of about 15.75% and 32.62% at the age of 7 days. In addition, as in Fig. 14 the relation between split tensile strength and TRCA replacement was found to be significant with 0.81 and 0.82 R^2 values.

Performance of TRCA-CA75-FA75-2 with UCCNA prioritized binder was found to be neutral. Specifically, the relative performance of TRCA-CA75-FA75-2-UCCNA5 and TRCA-CA75-FA75-2-UCCNA10 was found to be nil.

Performance of TRCA-CA75-FA75-2 with CCNA prioritized binder was found to be enhanced. TRCA-CA75-FA75-2-CCNA15 was found to be optimal performed SCC mix. Simultaneously, the relation between split tensile strength and CCNA or UCCNA replacement was found to be less significant with 0.76 and 0.85 R^2 values.

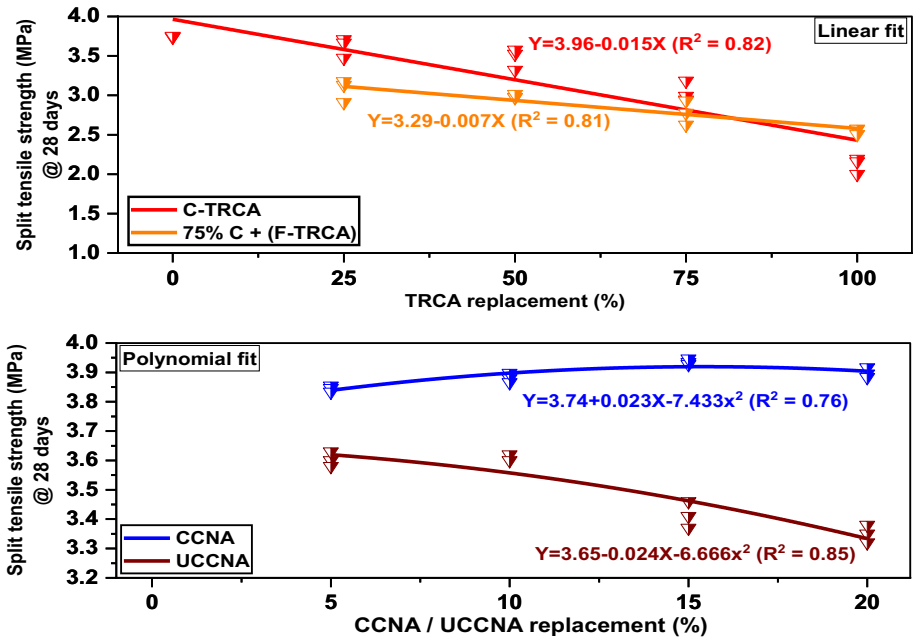

Fig. 14 Regression fit for split tensile strength of SCC

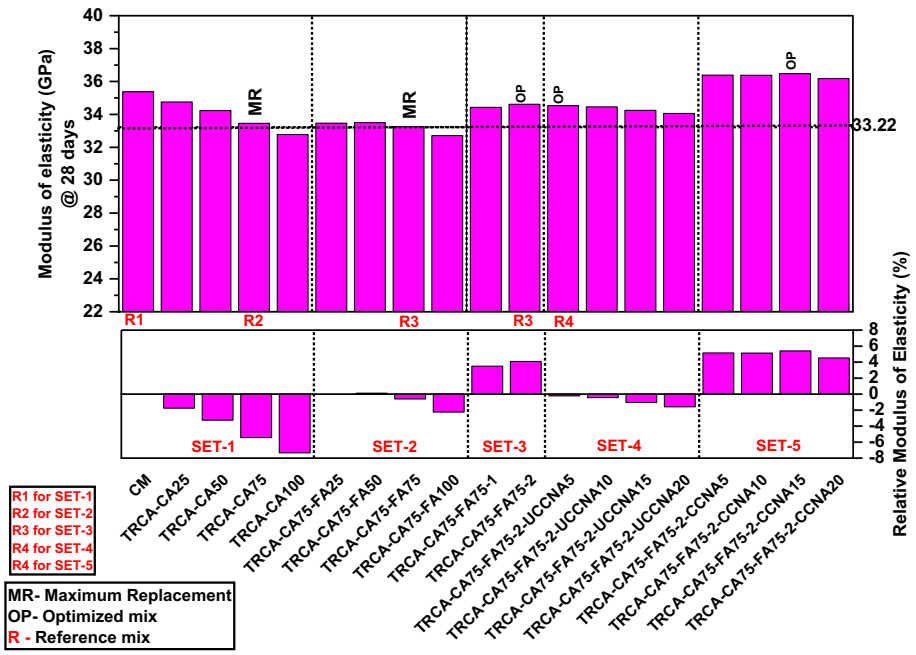

Fig. 15 Modulus of elasticity of SCC

Modulus of elasticity of SCC

The elasticity of concrete represents a decremental trend as the increase of TRCA replacement percentage as in Fig. 15. These results are in line with compression, flexural, and split tensile strength characteristics of concrete. The presence of adhering mortar around the TRCA improves the brittleness property of overall SCC, which results in poor elasticity [85]. Still, most of the TRCA-based SCC were succeeded to fulfil the compliance requirement except TRCA-CA100 and TRCA-CA75-FA100. In the context of BAGT, it was found that restriction of 1.18 mm or less sized TRCA became beneficial for the improvement of relative modulus of elasticity of about 4.01%, regards TRCA-CA75-FA75-2 SCC mix. Furthermore, as in Fig. 16 the linear relation between modulus of elasticity and TRCA replacement was found to be significant with 0.98 and 0.80 R^2 values.

Elasticity performance of TRCA-CA75-FA75-2 in the presence of UCCNA was found to be neutral (less than 0.43% relative modulus of elasticity were observed) regards 5% and 10% replacement levels. Further UCCNA

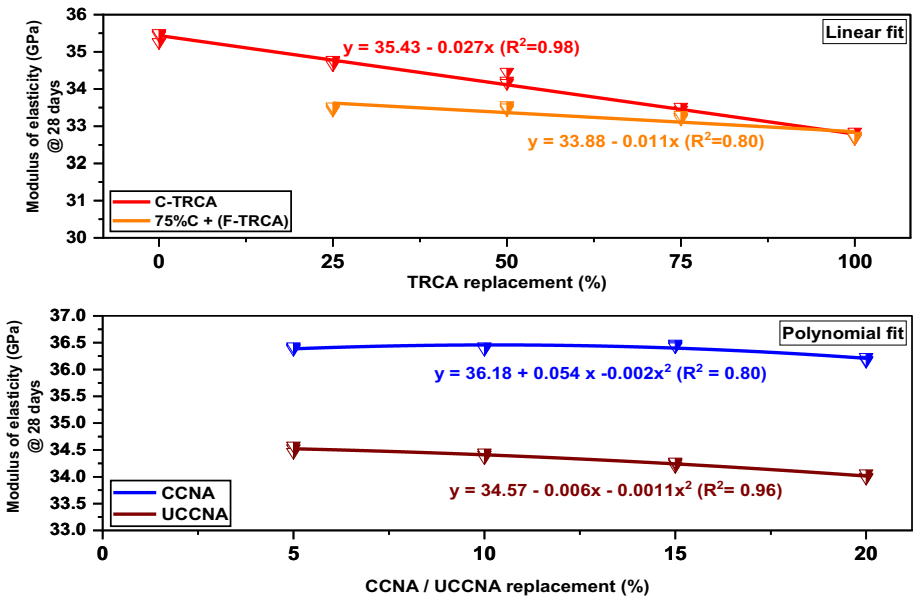

Fig. 16 Regression fit for split tensile strength of SCC

replacement, specifically at 15% and 20%, imparted a reduction of − 1.04% and − 1.68% of relative modulus of elasticity. However, all UCCNA-based SCC mixes were succeeded to fulfil the compliance requirements.

Besides the elasticity, the behaviour of TRCA-CA75-FA75-2 in the presence of CCNA was found to be incremental up to 15%, though relative modulus of elasticity was found to be similar and was about in and around 5%. At 20% CCNA, a decremental trend regards relative modulus of elasticity was observed. Altogether, retains between modulus of elasticity and CCNA or UCCNA replacement were found to be significant with 0.860 and 0.96 R^2 values.

SEM examination of SCC binders

Microstructure images of OPC, binary, and ternary pastes were taken with a working distance of about 2.3–4.2 mm, and lower voltages (5 kV) were used to avoid charging disturbances. Each microstructure image was taken with a magnification of 10 kx at the age of 7- and 90-day curing period. Observation OPC at the age of 7 and 90 days (Refer Figs. 17a and 18k) revealed calcium-depleted paste with a new class of microcracks, which appeared due to the heat of hydration [86]. This is due to un-hydrated calcium hydroxide platelets in the concrete matrix, as well as small CSH fibres that cover the anhydrous calcium silicate grains of calcium silicate [37, 87]. It demands supplementary pozzolanic materials to compensate for microcracks, and at present, the addition of FFA as a partial replacement to OPC fulfils the demand. FFA generally consists of Al, Si, and K (as in Fig. 1) with an average particle size of about 9 µm (as in Fig. 2b). FFA probably adsorbs Ca ion at an early hydration age, which gives an appearance of a microcrack-free structure by minimizing the gap (0.5–1 µm) between CH crystals parallel to the cleavage plane was often observed [86].

A ternary combination of pastes was examined with UCCNA and CCNA as a prominent constituent ingredient. Observation revealed the presence of un-hydrated FFA in the ternary paste at the age of 7 days. However, in the context of UCNNA and CCNA, the growth of hydrated products attached with un-hydrated FFA was only observed in CCNA prominent ternary binders. Specifically, these observations were found for OPC+FFA+CCNA5 (Fig. 17g), OPC+FFA+CCNA10 (Fig. 17h), and OPC+FFA+CCNA20 (Fig. 17i), in comparison with OPC+FFA+UCCNA5 (Fig. 17c), OPC+FFA+UCCNA10 (Fig. 17d), and OPC+FFA+UCCNA20 (Fig. 17e) at the age of 7 days. The presence of unburnt carbon (evident by TGA performance of UCCNA as in Fig. 2c) in UCCNA is the reason for the detachment between hydrated products and un-hydrated FFA at the age of 7 days. Because these unburnt carbons retard the reaction phase, which results in a porous structure. In the context of rheological properties of SCC, it was found to be advantageous, and it became an evident reason for the increment of slump flow properties of UCCNA-based SCC mixes in comparison with CCNA-based SCC mixes as discussed in Sect. 4.1 (refer Fig. 8).

Further observation of hydrated product at the age of 90 days revealed the presence of un-hydrated FFA in UCCNA prominent binders. It represents poor paste structure with less CSH (calcium silicate hydrate), CH (calcium hydroxide), and ettringite at the age of 90 days. It was evident for the reduction of mechanical properties of UCCNA-based SCC mixes. Simultaneously, more CH and ettringite formation was observed in OPC+FFA+UCCNA5

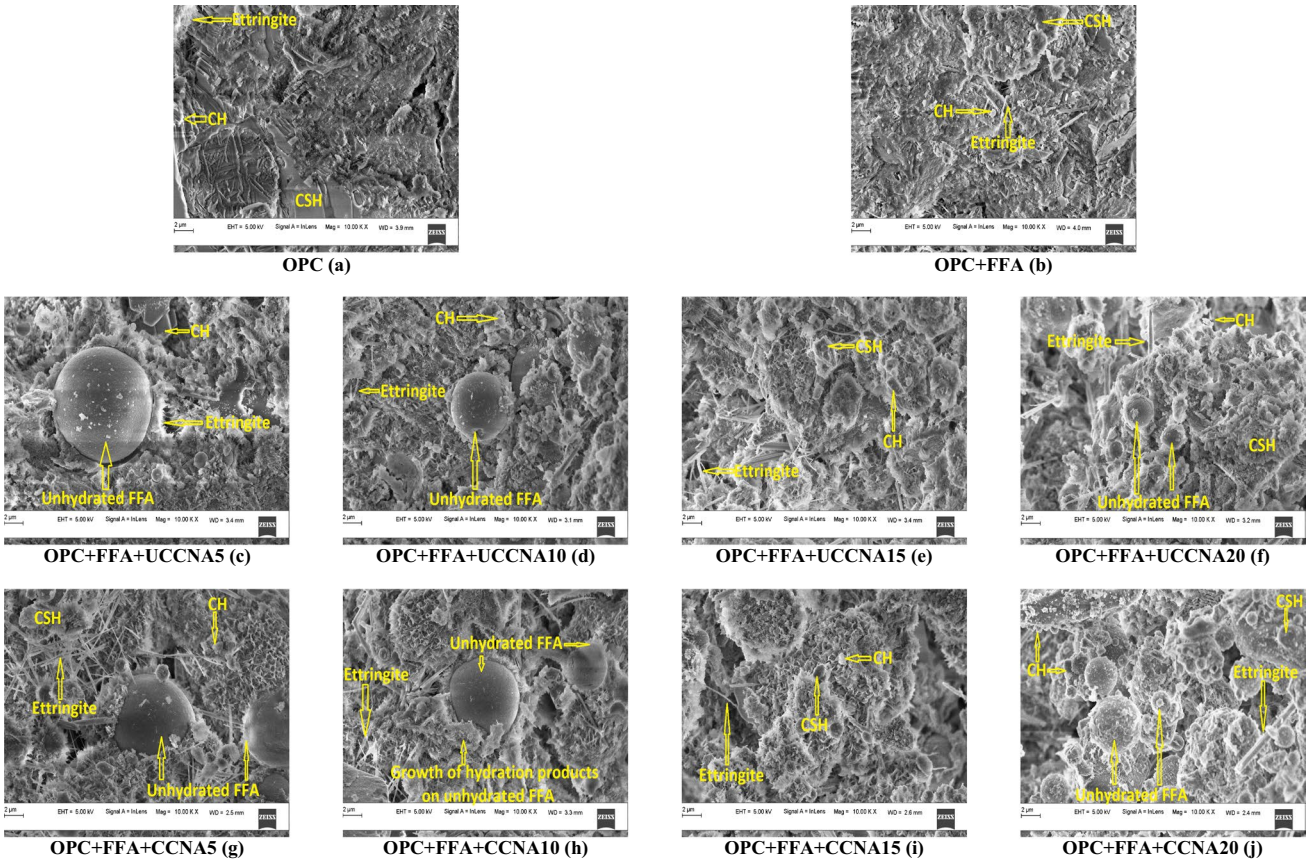

Fig. 17 FE-SEM images of binders at the age of 7 days

(Fig. 18m) and OPC+FFA+UCCNA10 (Fig. 18n) at the age of 90 days, which represents durability challenges of ternary paste [88]. Further, UCCNA prominent binders like (OPC+FFA+UCCNA15 (Fig. 18o) and OPC+FFA+UCCNA20 (Fig. 18p) represent more unhydrated FFA with a pore structure. However, in the context of CCNA prominent binders, dense structures with well-hydrated products of CSH, CH, and ettringite were observed at the age of 90 days. Overall, in comparison with all paste combinations, OPC+FFA+CCNA15 (Figs. 17i and 18s) were found to be dense with well-formed hydrated products at age of both 7 and 90 days of curing periods. Additionally, these findings are in line with the mechanical and rheological properties of SCC.

EDS examination of SCC binders

Energy-dispersive spectroscopy detailed analysis of OPC, binary, and ternary binders is presented in Table 5. Si, Al, and Ca are major identified elements. The increased UCCNA content in ternary binder decrement trend regards Ca and Si+Al was found; it might be due to the increase of unburnt carbon in overall UCCNA prominent ternary blends [58]. These findings are in line with SEM analysis, where detachment between hydrated products and unhydrated FFA was observed at the age of 7 days (Fig. 17). Further, with the context of CCNA, an increment of Ca and Si+Al with an increase of CCNA replacement percentage (up to 15%) was found. However, at OPC+FFA+CCNA20, decremental element constituents were identified (Ca and Si+Al). It revealed that reaction degree performance of CCNA with OPC and FFA was found to be optimal at 15%. Further replacement of CCNA reduced the reaction degree performance with OPC and FFA; it might be due to the appearance of imbalance regards to shape, texture, and presence of unburnt carbon in the form of agglomerates in CCNA [37, 58], which resulted in decrement of Ca and Si+Al constituents. These findings were in agreement with identified dense structure as observed in SEM images at the age of 90 days (Fig. 18).

Elements ratios like Ca/Si, Ca/(Si+Al), Si/Al, and Ca/Al are having a strong relation with mechanical characteristics of SCC. Specifically, Ca/Si and Si/Al have proportional and inversely proportional relation with the compressive strength of SCC [37, 89]. Figure 19 represents the relation of compressive strength versus element ratios. In the context

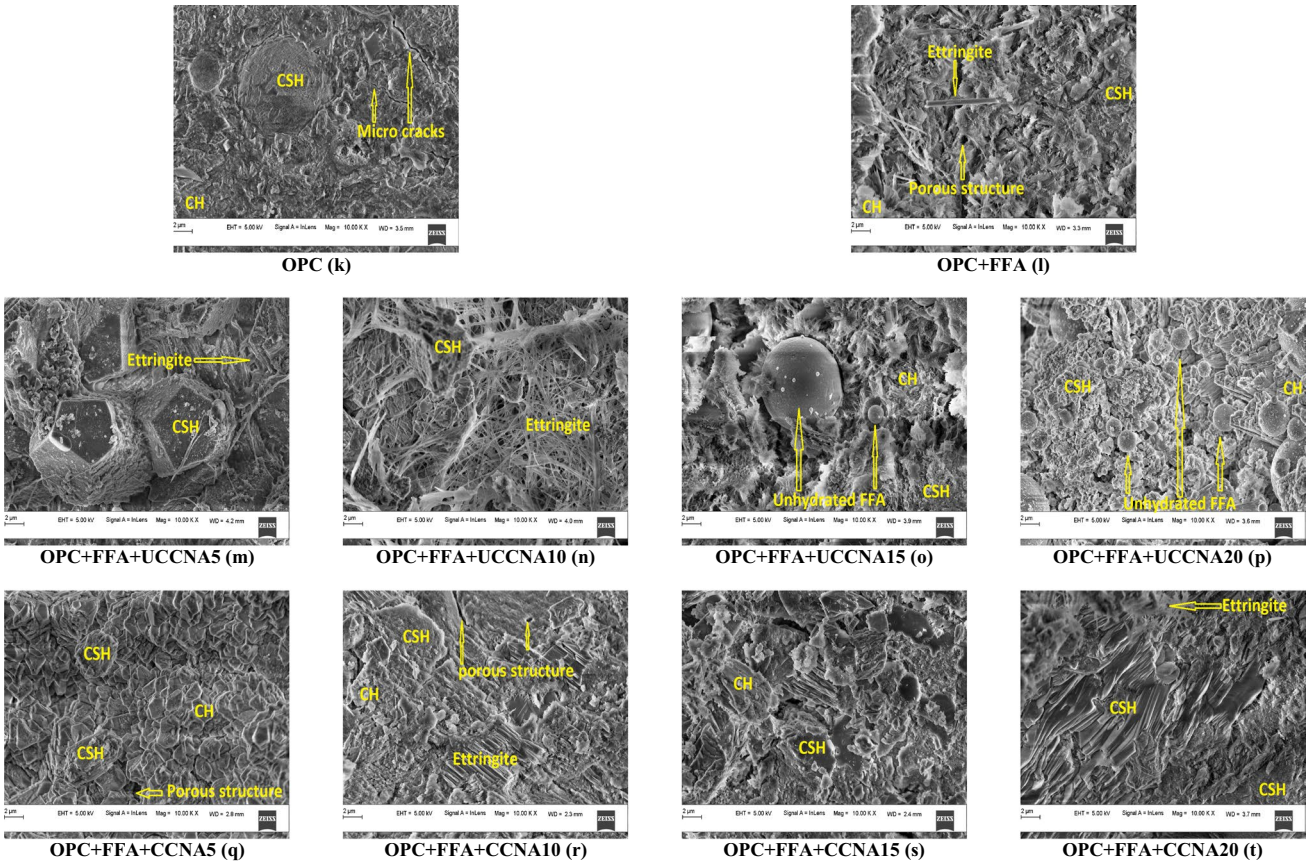

Fig. 18 FE-SEM images of binders at the age of 90 days

of UCCNA, decremental compressive strength was proportional and inversely proportional to Ca/Si and Si/Al ratios, respectively. Further, with CCNA context, incremental compressive strength was proportional and inversely proportional to Ca/Si and Si/Al ratios, respectively.

It was due to the incremental of additional CSH gels in the presence of CCNA up to 15% replacement. Besides, the maximum Ca/Si ratio of about 2.12 (at the age of 7 days) and 2.931 (at the age of 90 days) with minimal Si/Al ratio of about 2.102 (at the age of 7 days) and 2.955 (at the age of 90 days) was found for OPC+FFA+CCNA15. The discoveries of higher Ca/Si ratios and lower Si/Al ratios have been attributed to the formation of more CSH gel [37, 90]. Simultaneously identified CSH gels by TGA and XRD examination are in line with EDS findings. Overall OPC+FFA+CCNA15 was found to be an optimal performed ternary combination. In addition, these findings are even in line with the mechanical properties of SCC. Simultaneously, identified CSH gels by TGA and XRD examination were in line with EDS findings. Overall OPC+FFA+CCNA15 was found to be an optimal performed ternary combination. In addition, these findings were in line with the mechanical properties of SCC.

TGA examination of SCC binders

Thermogravimetric was performed on OPC, binary (OPC + FFA), and ternary (as UCCNA and CCNA prominent) paste with a rated temperature of about 5 °C/min for 7 and 90 days of curing period as in Figs. 20 and 21. In the context of 7-day curing period (Fig. 20), Derive. weight (%) represents disturbance by having huge variation between 0.4 and − 1.2%, which represents a loose phase of paste structure. Simultaneously at 90-day curing period (Fig. 21), Derive. weight (%) represents minimal disturbance by having the least variation between − 0.016 and − 0.16%, which represents a dense phase of paste structure. These findings are well in agreement with the SEM characterization of paste. Initial loss of weight was found between 49–191 °C and 46–218 °C for 7- and 90-day curing period. In this, loss of H_2O was due to dehydration of CSH as a major chemical component followed by carboaluminates and ettringite as a secondary chemical component [91, 92]. The second major weight loss was observed between 332–441 °C and 353–468 °C for 7- and 90-day curing period. This major weight loss corresponds to the dehydroxylation of portlandite (CH) [93, 94]. The

Table 5 EDS analysis of SCC binder pastes

Mixes	Si	Al	Ca	Si+Al	Si/Al	Ca/(Si+Al)	Ca/Si	Ca/Al
At the age of 7 days								
OPC	6.150	2.560	9.560	8.710	2.402	1.098	1.554	3.734
OPC+FFA	6.260	2.530	9.510	8.790	2.474	1.082	1.519	3.759
OPC+FFA+UCCNA5	6.070	2.620	9.260	8.690	2.317	1.066	1.526	3.534
OPC+FFA+UCCNA10	5.640	2.330	8.380	7.970	2.421	1.051	1.486	3.597
OPC+FFA+UCCNA15	5.350	2.160	7.780	7.510	2.477	1.036	1.454	3.602
OPC+FFA+UCCNA20	5.280	2.060	7.540	7.340	2.563	1.027	1.428	3.660
OPC+FFA+CCNA5	5.310	1.860	9.060	7.170	2.855	1.264	1.706	4.871
OPC+FFA+CCNA10	5.330	2.140	10.050	7.470	2.491	1.345	1.886	4.696
OPC+FFA+CCNA15	5.340	2.540	11.320	7.880	2.102	1.437	2.120	4.457
OPC+FFA+CCNA20	5.680	2.150	9.010	7.830	2.642	1.151	1.586	4.191
At the age of 90 days								
OPC	5.112	1.730	14.880	6.842	2.955	2.175	2.911	8.601
OPC+FFA	4.450	1.290	11.563	5.740	3.450	2.014	2.598	8.964
OPC+FFA+UCCNA5	5.156	1.623	10.800	6.779	3.177	1.593	2.095	6.654
OPC+FFA+UCCNA10	5.270	1.550	10.520	6.820	3.400	1.543	1.996	6.787
OPC+FFA+UCCNA15	5.660	1.530	10.460	7.190	3.699	1.455	1.848	6.837
OPC+FFA+UCCNA20	5.712	1.352	9.380	7.064	4.225	1.328	1.642	6.938
OPC+FFA+CCNA5	5.011	1.160	14.023	6.171	4.320	2.272	2.798	12.089
OPC+FFA+CCNA10	5.030	1.440	14.260	6.470	3.493	2.204	2.835	9.903
OPC+FFA+CCNA15	5.200	1.760	15.240	6.960	2.955	2.190	2.931	8.659
OPC+FFA+CCNA20	5.350	1.510	15.628	6.860	3.543	2.278	2.921	10.350

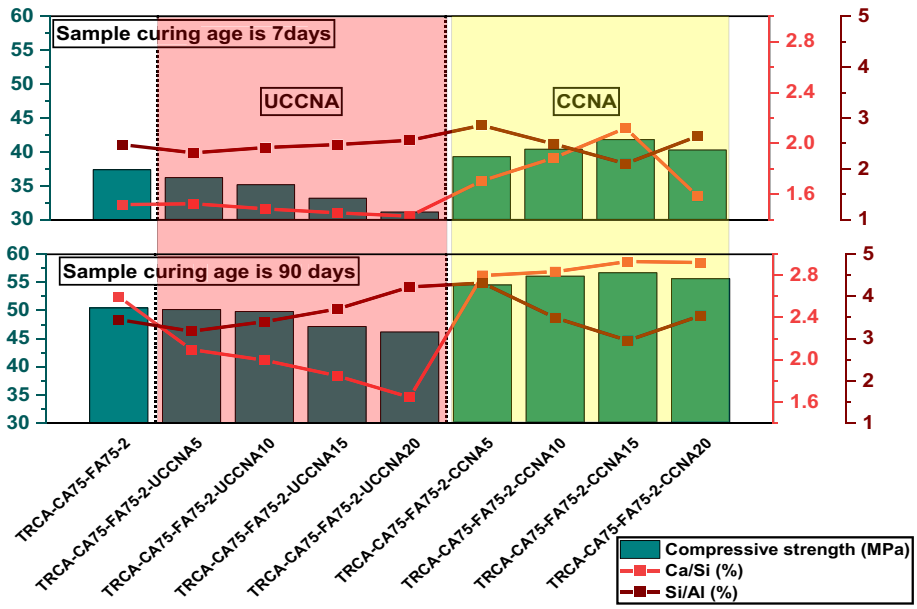

Fig. 19 Relation between compressive strength versus Ca/Si versus Ca/Al

third major weight loss was found between 575–674 °C and 583–700 °C for 7- and 90-day curing period. This huge loss corresponds to the decarbonization of calcium carbonate coming from the clinker and the filler [91, 95]. Beyond 700 °C, weight loss was found to be neutral, because of the irreversible chemical component exhibited by the binder test subjects. In the context of UCCNA and CCNA ternary binders, major weight loss was observed in CCNA prioritized binders rather than UCCNA prioritized binders at the age of 7- and 90-day curing periods. CCNA was found to be more productive regards the production of CSH, CH, and ettringite which results in a denser structure rather than UCCNA prioritized binder.

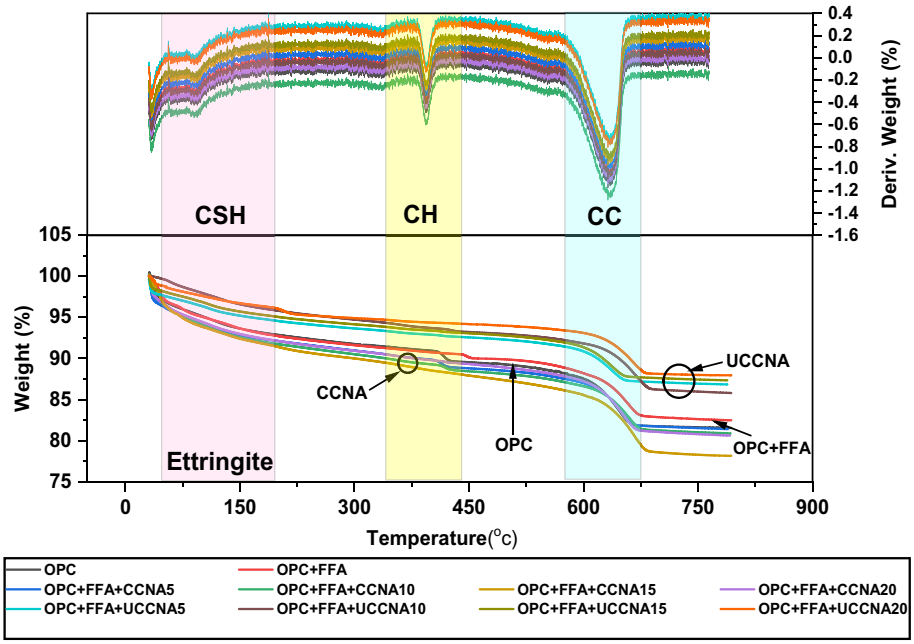

Fig. 20 Thermogravimetric analysis on pastes at 7-day curing period

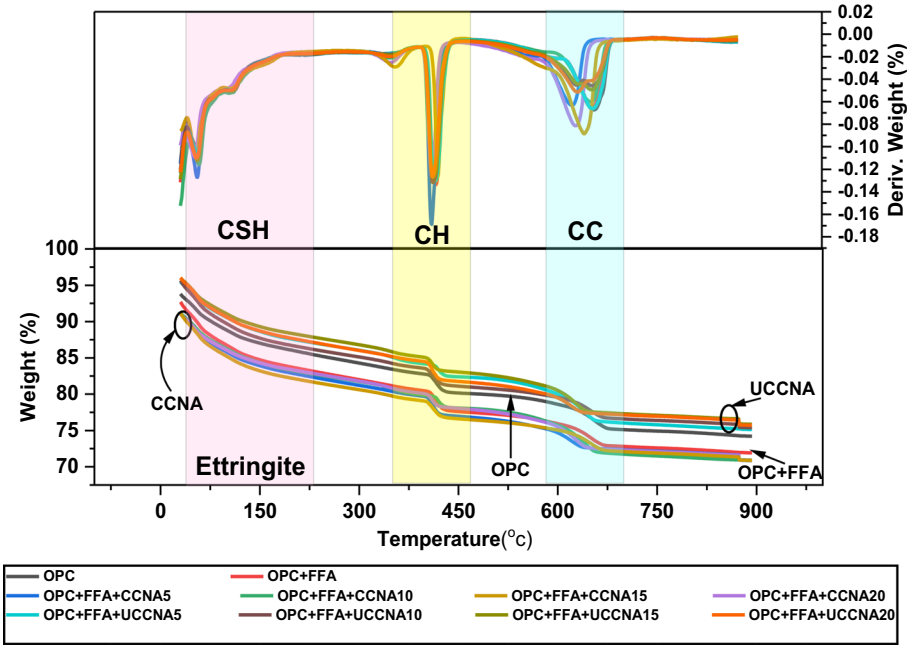

Fig. 21 Thermogravimetric analysis on pastes at 90-day curing period

Specifically, OPC+FFA+CCNA15 (weight loss of about 96–78% and 91–70% at the age of 7 and 90 days) was found to be in optimal combinations, which represent major weight loss regards 7- and 90-day curing period. These findings are in line with mechanical properties, XRD, and FTIR findings of SCC. OPC+FFA+UCCNA15 and OPC+FFA+UCCNA20 were found to be poor ternary combinations by gaining the least weight loss of about 99–87% and 95–75% at the age of 7 and 90 days. It confirms the presence of less quantified CSH, CH, and ettringite. Overall UCCNA replacement reduces the contribution of hydrated products in cement paste. Simultaneously CCNA replacement was found to be beneficial by contributing additional CSH gels.

XRD examination of SCC binders

Figures 22 and 23 illustrate XRD analysis of OPC, binary, and ternary pastes at the age of 7 and 90 days. Clinotobermorite (CSH), portlandite (CH), ettringite (E), and calcite (C) were found to be major phases regards all types of OPC, binary, and ternary pastes. Table 6 represents

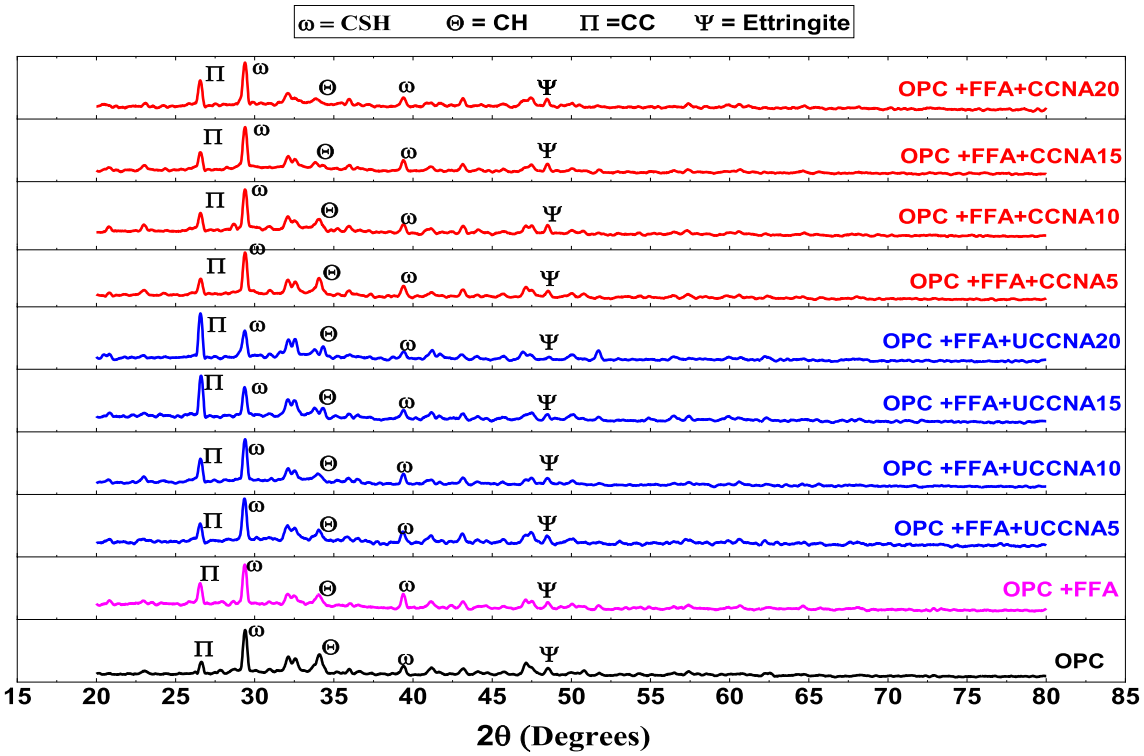

Fig. 22 XRD analysis on pastes at 7-day curing period

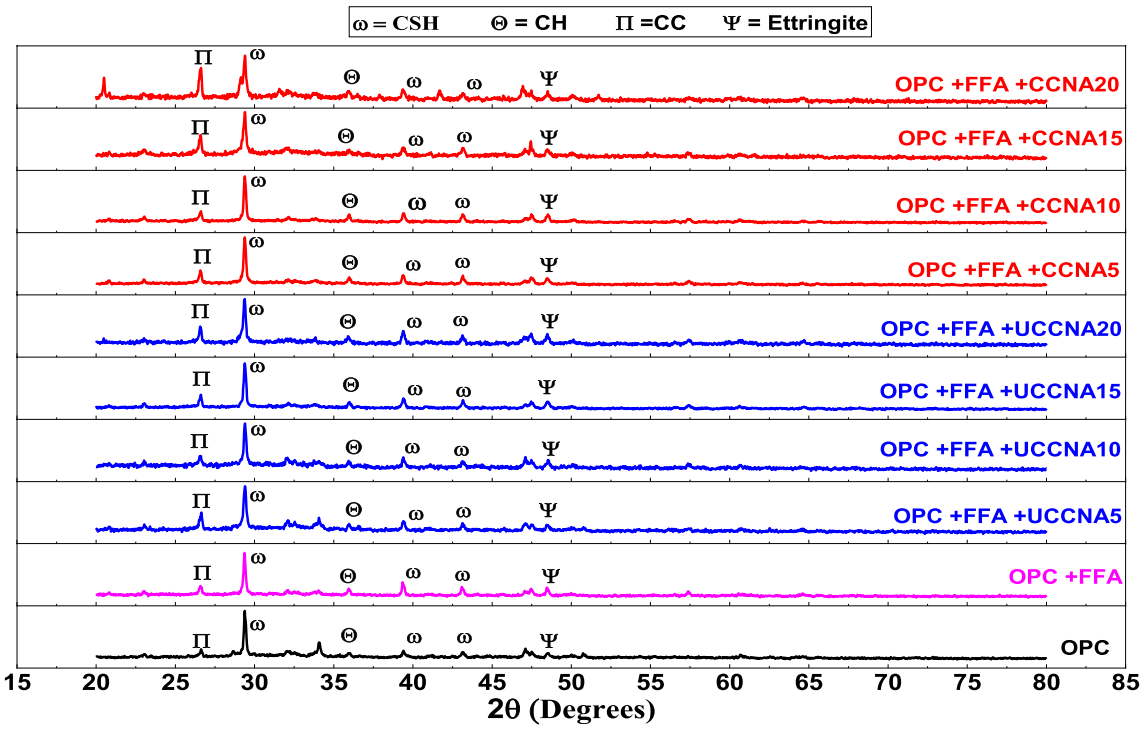

Fig. 23 XRD analysis on pastes at 90-day curing period

Table 6 Identification of the compound name and chemical formula of pastes

Identity	Ref. code	Compound name	Chemical formula
CSH	96-100-0047	Clinotobermorite	$Ca_5Si_6O_{18}H$
CH	96-900-0113	Portlandite	$Ca_1O_2H_2$
E	96-901-2923	Ettringite	$Ca_{12}A_{l4}S_6O_{100}H_{128}$
CC or $CaCO_3$	96-900-9668	Calcite	$Ca_6C_6O_{18}$

identified compounds and the chemical formulae of the same. Changes in peak heights and the formation of new peaks were identified through XRD analysis at the age of 90 days. The intensity of alite and belite was decreased and a new peak of clinotobermorite (CSH) was found at the age of 90 days (two thetas deg. 43 as in Fig. 23). Moreover, an increase in peak heights was observed regards ternary pastes validated the formation of intensified crystalline phase due to the addition of CCNA. Even these findings are in line with SEM, EDS, and TGA analysis. Further quantification of compounds was measured through XRD analysis and compared with compressive strength characteristics of concrete as in Fig. 24. The percentage quantification of these compounds was identified as a function of the paste phase, concentration, and the relationship between the intensity of the peak and the weight fraction. It was found that as the CSH quantification percentage increases, an increase regards compression strength was observed for CCNA prioritized binders. Meanwhile, with the decrease of CSH quantification percentage, a decrease regards compression strength was observed for UCCNA prioritized binders. The presence of more unburnt carbon in UCCNA was the cause for the reduction of clinotobermorite (CSH) gel resulting in poor structure. It is supported by TGA findings as in Figs. 20 and 21. Moreover, quantification of CSH, CH, CC, and E varies between 48–66%, 1–7.9%, 7–19.8%, and 15–34%, respectively. Observation of CH, CC, and E in comparison with compression strength was found to be insignificant. These findings is evident that the addition of CCNA was found to be advantageous, which implicates the dense structure. It was found that a maximum of up to 66% of CSH gels contributed to the formation of dense paste structures concerning the OPC+FFA+CCNA15 combination.

FTIR examination of SCC binders

Vibration frequencies of OPC, binary, and ternary pastes at the age of 7 and 90 days were measured by FTIR as in Fig. 25. Identifications give a sign of change in silicate, sulphate, hydroxide, and carbon phases. Silicate condensation reaction was observed through silicate infrared bands. Si–O bending (v_4 of SiO_4) was characteristically found at wavenumber 656 cm^{-1} [96, 97]. Here sulphate chemistry displays very rapid crystallization followed by a slow recrystallization phase [98]. The percentage transmittance was found to be decreased for OPC, binary, and ternary pastes at the age of 90 days. The bending at 714 cm^{-1}, 877 cm^{-1} due to v_4 of CO_3 and v_2 of CO_3 was observed [99–101]. The development of a drop feature in the spectra at 800–970 cm^{-1}, qualified as the dissolution of C_3S alite, correlates with the formation of CSH. The presence of a wide-ranging absorption hump between 995 and

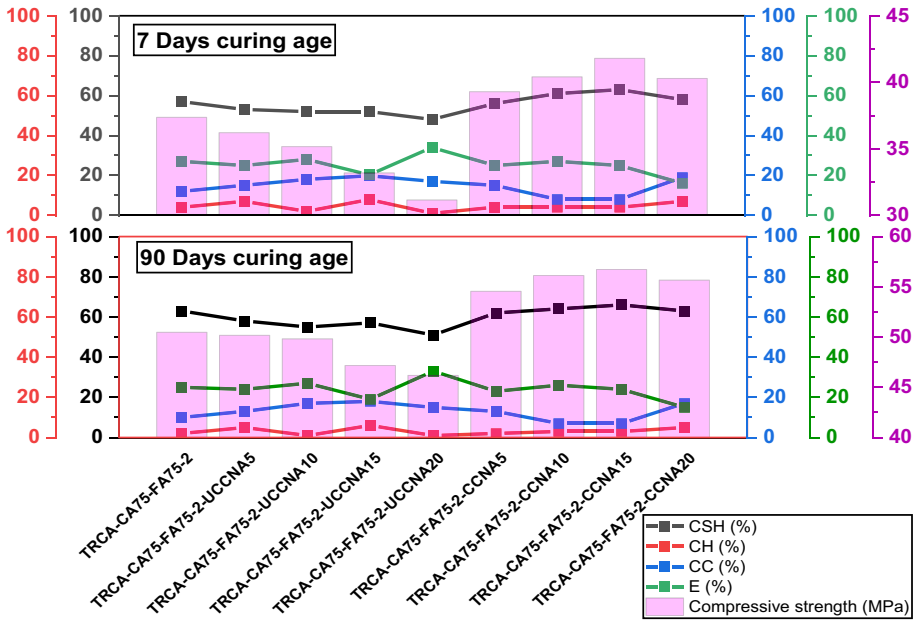

Fig. 24 XRD quantification versus compressive strength

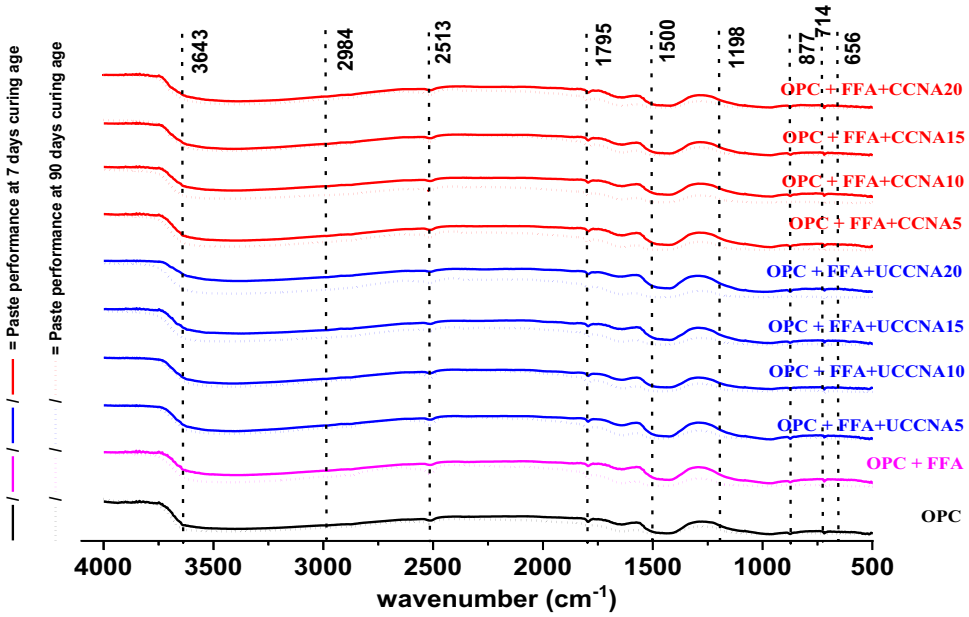

Fig. 25 FTIR analysis on pastes at 7- & 90-day curing periods

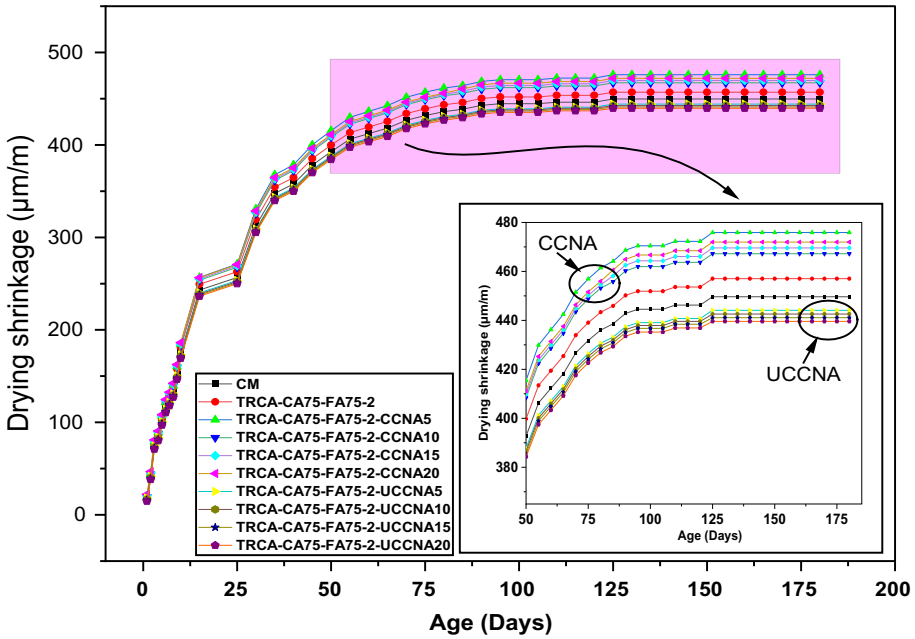

Fig. 26 Drying shrinkage examination on SCC

1100 cm^{-1} might be due to polymeric silica. It was associated with the growth of water bending vibration bands (1500 cm^{-1}1795 cm^{-1}). This implies the formation of calcium silicate hydrate, CSH [98]. These findings were in line with XRD, TGA, and SEM observations as discussed in Sects. 4.6 and 4.7. Moreover, O–H bends were observed at 1618 cm^{-1}–1686 cm^{-1} due to gypsum, syngenite, and anhydrite minerals [99]. Identified wavenumber frequency at 1198 cm^{-1} and 1500 cm^{-1} is due to v_3 of SO_4 and CO_3 [100, 101]. Further presence of $CaCO_3$ was confirmed at 1795 cm^{-1} and 2513 cm^{-1} [98, 99]. At higher frequency, precisely at 3643 cm^{-1} presence of calcium hydroxide ($Ca(OH)_2$) was confirmed [98, 99]. The hydrated minerals have unique signatures due to O–H stretching and bending vibrations regards UCCNA and CCNA prioritized binders. The spectrum of the UCCNA and CCNA prioritized binders distinct features regards the hydroxides of calcium and magnesium, which have distinct O–H stretching frequencies and calcium carbonate has characteristic fundamentals and overtones well separated from the sulphate bands [99]. Overall finding results reveal that densified paste structure was formed with regard to the CCNA prioritized binders in confidence with XRD, TGA, and SEM findings, and it was moreover contributed by the formation of additional

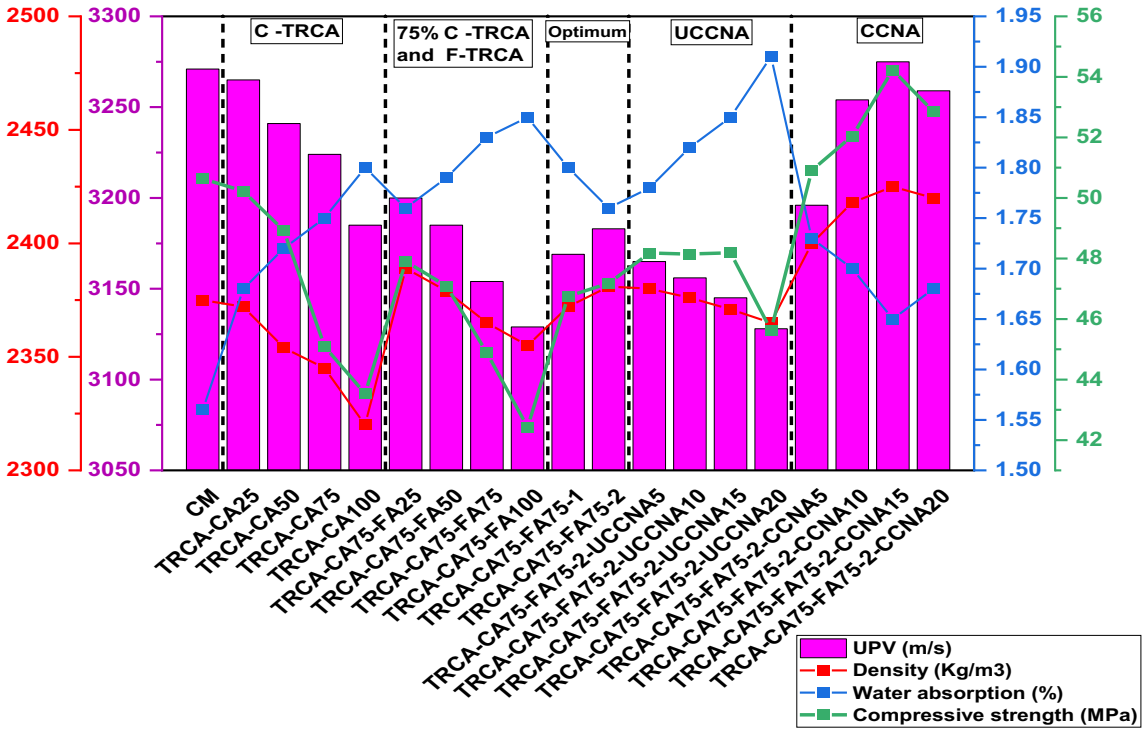

Fig. 27 Quality assessment of SCC at the age of 28 days

CSH gels which purely depended on well-balanced ratios of sulphates and C_3A+C_4AF [98].

Drying shrinkage examination of SCC

Drying shrinkage performance on CM (base), TRCA-CA75-FA75-2 (to analyze the TRCA dominance), UCCNA and CCNA priority-based SCC mixes is presented in Fig. 26. Loss of water causes a change in length and volume due to self-desiccation and evaporation termed as shrinkage. The rate of shrinkage tends to be higher at the beginning of duration up to the age of 50 days and later stage shrinkage diminished. The magnitude of drying shrinkage was fewer regards UCCNA prioritized blends; simultaneously, a higher magnitude was found regards CCNA prioritized blends. The presence of more unburnt carbon in UCCNA reduces the rate of hydration and the overall degree of chemical reaction as confirmed by XRD, FTIR, TGA, SEM, and EDS findings. In addition, particle size distribution represents a coarser structure as in Fig. 2b than CCNA and FFA, which was the reason for less magnitude of drying shrinkage. Simultaneously, a higher degree of chemical reaction as confirmed by microstructural findings accelerates the hydration process, resulting in more demand regards to water, which promotes the higher magnitude of drying shrinkage. Besides the pozzolanic reaction of CCNA causes pore refinement that results in a greater rate of drying shrinkage [102]. Comparison of CM with TRCA-CA75-FA75-2 revealed that replacement of TRCA increases the water demand due to more WA characteristics of TRCA aggregate as confirmed in Fig. 7 resulting in more reduction regards concrete volume that results in greater drying shrinkage. Overall drying shrinkage was significantly increased due to CCNA and at the same; its behaviour was found to be vice-a-versa regards UCCNA prioritized blends.

Quality performance of SCC regards UPV, density, and water absorption

Performance evaluation through UPV represents modest characterization of SCC mixes by achieving velocity between 3121 and 3270 m/s. The compressive strength and density characteristics of SCC mixes were proportional to UPV performance. Simultaneously, WA characteristics of concrete were inversely proportional to UPV characteristics regards.

TRCA, UCCNA, and CCNA prioritized SCC blends. It was found that as the increase of TRCA replacement percentage decreased regards compressive strength, UPV, and density were observed. TRCA and UCCNA prioritized SCC blends impart more microcracks, which results in poor UPV performances. Moreover, a decrease regard compressive

Table 7 CO_2 emission factors for cementitious materials

Material	Energy requirements for 1000 kg				Transportation of 1000 kg		Total emission (kg CO2/kg)
	Consumption (kWh)			Emission factor (Kg CO_2/kWh) [105]	Distance (Km)	Emission factor (kg CO_2/km) [105]	
	Drying	Grinding/Sieving	Calcination				
FFA	26	134.2	–	0.521	100	0.192	0.1027
UCCNA	26	174.6	–	0.521	100	0.192	0.1240
CCNA	26	174.6	12	0.521	100	0.192	0.1300

strength and density were identified. However, concerning TRCA-CA75-FA75-1 and TRCA-CA75-FA75-2 improvements in compressive strength, density, and UPV performances were identified. It clarifies that BAGT with the restriction of 1.18 mm less sized fraction or so improves the SCC integral structure and was found to be advantageous. For that reason, an increase regards UPV performance of about 29 m/s was identified. Furthermore, CCNA prioritized SCC blends densified the mortar and it was evident by UPV, density, and compressive strength characteristics. Overall as per physical characteristics, it was found that replacement of 15% CCNA for the OPC was found to be optimal. Besides, quality assessment was in agreement with mechanical and microstructural findings (Fig. 27).

Carbon dioxide (CO_2) emissions

In the present study, CO_2 emission factors were analyzed by estimating the emission during the preparation of FFA, UCCNA, and CCNA, which include transportation, drying, grinding, calcination, and sieving process. Elaborated CO_2 emission factors of cementitious materials are presented in Table 7. Besides, Fig. 28 represents the CO_2 emission of major ingredients used in all SCC mixes. Comparison of ingredients revealed that OPC is the major source of CO_2 emission factor followed by CCNA, UCCNA, FFA, CA, TRCA-CA, TRCA-FA, and FA. Further, as a concrete composite, it was revealed that CM has the highest CO_2 emission rate of about 429.93 kg CO_2/m^3, while lowest CO_2 emission rate of about 346.50 kg CO_2/m^3 was found for TRCA-CA75-FA75-2-UCCNA20, and it was about a 19.41% reduction in comparison with CM. Replacement of natural aggregate with TRCA reduces the emission by 4.83% regards TRCA-CA75-FA75-2 mix in comparison with CM [103] and [104] findings revealed that switch of natural aggregate by TRCA directs towards a reduction in CO_2 emission by about 2% to 7%. However, the advantage of utilizing TRCA with CCNA or UCCNA sumped up in the conservation of natural resources despite its meagre contribution to lowering CO_2 emissions as validated in Table 8.

Figure 29 represents the efficiency of SCC concerning compressive strength and CO2 emissions at the age of 7 and 90 days. Regarding the efficiency of SCC mixes, replacement of TRCA to natural aggregate was found to be inefficient, precisely while comparing TRCA-CA75-FA75-2 with CM found efficiency reduction of about 3.18% and 2.38% at the age of 7 and 90 days. Further, efficiency was increased due to the replacement of OPC by UCCNA and CCNA. Regarding UCCNA maximum efficiency was gained by TRCA-CA75-FA75-2-UCCNA10 and was about 4.76% in comparison with CM at the age of 90 days. Simultaneously, regarding CCNA, maximum efficiency was gained by TRCA-CA75-FA75-2-CCNA20 and was about 23.011% and 26.98% in comparison with CM at the age of 7 and 90 days. It was evident that utilizing CCNA as an OPC replacement was found to be more advantageous in regard to the performance of concrete efficiency.

Conclusions

The present study focused on analyzing the performance of CCNA and UCCNA prioritized ternary blends in TRCA incorporated SCC. The performance of SCC mixes was analyzed in detail through measured rheological and mechanical properties. Besides, the microstructural performance of OPC, binary, and ternary blends was examined through SEM, EDS, XRD, TGA, and FTIR tests. In addition, the quality and dynamic instability of SCC were examined through UPV and drying shrinkage examinations. Based on overall findings following conclusions were drawn.

- Material characterization of UCCNA reveals coarser structure as of OPC. Besides TGA, performance ensures the presence of more unburnt carbons, but still, oxide composition classifies UCCNA as a pozzolanic material.

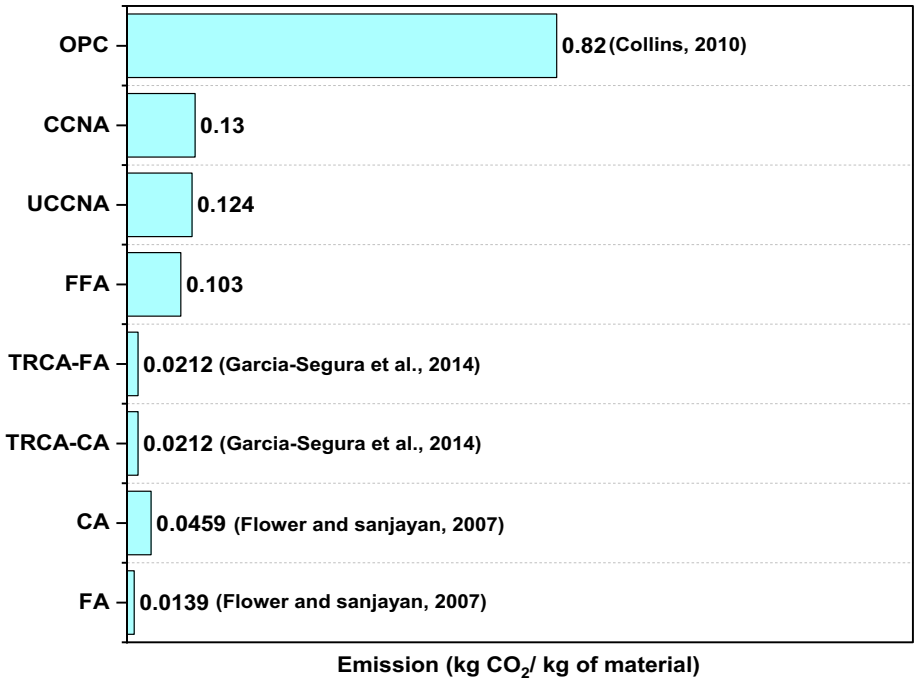

Fig. 28 CO_2 emission of major ingredients used in all SCC mixes

Table 8 CO_2 emissions for one cubic meter of SCC

Mixes	CO2 emissions for one cubic meter of concrete (kg CO_2/m^3)								
	OPC	FFA	UCCNA	CCNA	CA	TRCA-CA	FA	TRCA-FA	Total
CM	369	15.45	–	–	35.34	–	10.14		429.93
TRCA-CA75-FA75-2	369	15.45	–	–	8.54	6.76	1.89	7.50	409.14
TRCA-CA75-FA75-2-UCCNA5	350.55	15.45	2.79	–	8.54	6.76	1.89	7.50	393.48
TRCA-CA75-FA75-2-UCCNA10	332.10	15.45	5.58	–	8.54	6.76	1.89	7.50	377.82
TRCA-CA75-FA75-2-UCCNA15	313.65	15.45	8.37	–	8.54	6.76	1.89	7.50	362.16
TRCA-CA75-FA75-2-UCCNA20	295.20	15.45	11.16	–	8.54	6.76	1.89	7.50	346.50
TRCA-CA75-FA75-2-CCNA5	350.55	15.45	–	2.93	8.54	6.76	1.89	7.50	393.62
TRCA-CA75-FA75-2-CCNA10	332.10	15.45	–	5.85	8.54	6.76	1.89	7.50	378.09
TRCA-CA75-FA75-2-CCNA15	313.65	15.45	–	8.78	8.54	6.76	1.89	7.50	362.57
TRCA-CA75-FA75-2-CCNA20	295.20	15.45	–	11.70	8.54	6.76	1.89	7.50	347.04

- Material characterization of CCNA reveals finer structure as of FFA, and oxide composition classifies CCNA as pozzolanic + cementitious material.
- The adapted novel freezing–thawing cyclic procedure followed by Los Angeles abrasion treatment was found to be an advantage by reducing WA percentage by 9% (initial) to 2.94% and 3.91% regards TRCA coarse and fine.
- Rheological properties are sensitive regards TRCA replacement percentage, and it significantly appears to be a reduced trend as the increase of TRCA replacement percentage.
- Adaptation of BAGT with the restrict of TRCA-FA having particle size 1.18 mm or less was found to be advantageous regards slump flow characteristics, which enhance the relative slump flow performance by 3.27%.
- UCCNA prioritized SCC blends represent enhanced rheological performances up to 10% replacement percentage because the presence of more unburnt carbon retards the initial state of hydration. But at further replacement percentage which up to 20% rheological performance was diminished due to uncertain particle fraction as found by particle size distribution analysis of UCCNA, which coarser the overall ternary binder.
- CCNA prioritized SCC blends represent diminished rheological performances because CCNA was a pozzolanic + cementitious material and it was in the calcined phase, which enhanced the initial state reaction, which results in an accelerated hydration process.
- Compliance requirement of concrete analyzed through compression, flexural, and modulus of elasticity char-

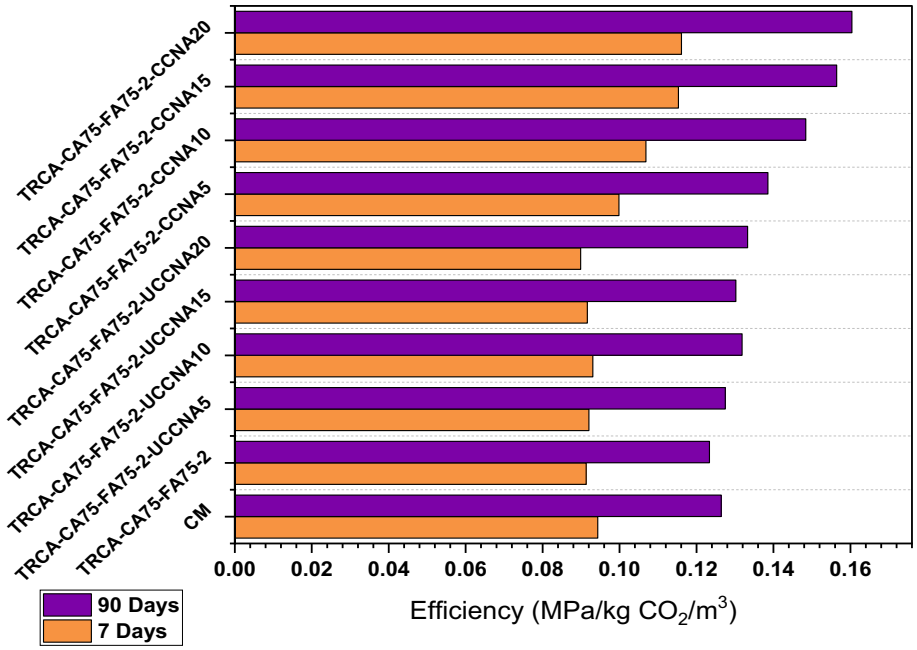

Fig. 29 The efficiency of SCC with respect to compressive strength and CO2 emissions

acteristics, and it revealed about possible maximum replacement percentage was up to 75% regards both TRCA coarse and fine aggregates.

- Mechanical characteristics of SCC decrease as the increase of replacement percentage regard the coarse and fines of TRCA. Besides BAGT was found to be a more suitable technique regards SCC mixes; specifically, restriction of 1.18 mm or less TRCA fraction through BAGT improves the relative performance of compressive, flexural, split, and modulus of elasticity strength by 19.11%, 31.12%, 32.15%, and 4.06%.
- UCCNA prioritized SCC blends represent decremental mechanical performance; simultaneously, CCNA prioritized SCC blends represent incremental mechanical performance up to 15%. The presence of more unburnt carbon was the culprit for the poor performance regards UCCNA prioritized SCC blends, and it was revealed that to bring reaction phase, calcination of agro-waste was essential.
- Microstructural findings regard SEM, EDS, XRD, TGA, and FTIR were in line with the rheological and mechanical performance of SCC mixes. It was found that 15% replacement of CCNA was optimal and UCCNA prioritized ternary blends represent poor reactive phase.
- Dynamic instability was analyzed through drying shrinkage, and it revealed that UCCNA prioritized SCC blends found to be more stable by gaining fewer shrinkage characteristics in comparison with CCNA prioritized SCC.
- Quality assessment of SCC through UPV represents dense structure regards CCNA prioritized SCC blends. Specifically, 15% of CCNA prioritized SCC represents fewer microcracks with the solidified integral structure of SCC.
- In terms of CCNA, the maximum efficiency was achieved with TRCA-CA75-FA75-2-CCNA20 and was around 23.011% and 26.98% compared to CM at 7 and 90 days of age.
- The lowest CO_2 emission rate of about 346.50 kg CO_2/m^3 was found for TRCA-CA75-FA75-2-UCCNA20, and it was about a 19.41% reduction in comparison with CM.

Overall utilization of UCCNA in the ternary blend was found to be unscientific, and it appeared to be drawback regards mechanical characteristics of concrete. However, at the same instant regards dynamic instability UCCNA was found quite beneficial. However, UCCNA is not recommended to use as a binder for real-time practices. Besides CCNA is recommended to utilize as a supplementary cementitious binder, specifically TRCA-CA75-FA75-2-CCNA15 is recommended for the application of field condition practices.

Acknowledgements The authors are thankful to the Department of Civil Engineering, Manipal Institute of Technology, MAHE, Manipal, Karnataka, India. The authors also express gratitude to Dr.Murari M S, Scientific Officer, DST-PURSE Program, Mangalore University, who facilitated us to perform FE-SEM and EDS, and also, extend our thanks to the department of chemical engineering and DAMP Manipal Institute of Technology for TGA, FTIR, and XRD facilities.

Funding Open access funding provided by Manipal Academy of Higher Education, Manipal.

Declarations

Conflict of interest The authors declare that they have no conflicts of interest.

Ethical statement The authors declare that they have not submitted the manuscript to any other journal for simultaneous consideration. The work is original and not published elsewhere.

References

1. Somarriba Sokolova LN, Ermakova EV, Rynkovskaya M (2018) A review of agro-waste materials as partial replacement of fine aggregate in concrete. IOP Conf Ser Mater Sci Eng. https://doi.org/10.1088/1757-899X/371/1/012012
2. Memon SA, Khan S, Wahid I, Shestakova Y, Ashraf M (2020) Evaluating the effect of calcination and grinding of corn stalk ash on pozzolanic potential for sustainable cement-based materials. Adv Mater Sci Eng. https://doi.org/10.1155/2020/1619480
3. He J, Kawasaki S, Achal V (2020) The utilization of agricultural waste as agro-cement in concrete: a review. Sustainability. https://doi.org/10.3390/SU12176971
4. Ramadhansyah PJ, Mahyun AW, Salwa MZM, Abu BBH, Megat JMA, Wan IMH (2012) Thermal analysis and pozzolanic index of rice husk ash at different grinding time. Proc Eng 50:101–109. https://doi.org/10.1016/j.proeng.2012.10.013
5. Ábrego J, Plaza D, Luño F, Atienza-Martínez M, Gea G (2018) Pyrolysis of cashew nutshells: characterization of products and energy balance. Energy 158:72–80. https://doi.org/10.1016/j.energy.2018.06.011
6. Givi AN, Rashid SA, Aziz FNA, Salleh MAM (2010) Assessment of the effects of rice husk ash particle size on strength, water permeability and workability of binary blended concrete. Constr Build Mater 24:2145–2150. https://doi.org/10.1016/j.conbuildmat.2010.04.045
7. Bie RS, Song XF, Liu QQ, Ji XY, Chen P (2015) Studies on effects of burning conditions and rice husk ash (RHA) blending amount on the mechanical behavior of cement. Cem Concr Compos 55:162–168. https://doi.org/10.1016/j.cemconcomp.2014.09.008
8. Rukzon S, Chindaprasirt P, Mahachai R (2009) Effect of grinding on chemical and physical properties of rice husk ash. Int J Miner Metall Mater 16:242–247. https://doi.org/10.1016/S1674-4799(09)60041-8
9. Ganesan K, Rajagopal K, Thangavel K (2008) Rice husk ash blended cement: assessment of optimal level of replacement for strength and permeability properties of concrete. Constr Build Mater 22:1675–1683. https://doi.org/10.1016/j.conbuildmat.2007.06.011
10. Saroj PL (2015) Advances in cashew production technology. http://www.cashew.res.in
11. Tipraj, Prasanna EL, Prabhanjan N, Krishna AS, Prasad MG (2018) Experimental study on strength of concrete by partial replacement of cement by nano silica and fly ash. Int J Civ Eng Technol 9:1763–1771
12. Paper C, Ara S, Gerais M (2010) Analysis of the cashew nut production I pro-Africa conference
13. Journal A, Sciences A (2015) Effect of water absorption and sorptivity of concrete with partial replacement of cement by cashew nut shell ash. Aust J Basic Appl Sci 9:311–316
14. Pandi K, Anandakumar R, Ganesan K (2019) Study on optimum utilisation of groundnut shell ash and cashew nut shell ash in concrete. Caribb J Sci 53:981–991
15. Oyebisi S, Igba T, Oniyide D (2019) Performance evaluation of cashew nutshell ash as a binder in concrete production. Case Stud Constr Mater 11:e00293. https://doi.org/10.1016/j.cscm.2019.e00293
16. Oyebisi S, Igba T, Raheem A, Olutoge F (2020) Predicting the splitting tensile strength of concrete incorporating anacardium occidentale nut shell ash using reactivity index concepts and mix design proportions. Case Stud Constr Mater 13:e00393. https://doi.org/10.1016/j.cscm.2020.e00393
17. Satpathy I, Malik JK, Arora N, Kapur S, Saluja S, Bhattacharjya S (2016) Material consumption patterns in INDIA: GIZ Report 2016 pp 1–161
18. Satpathy I, Malik JK, Arora N, Kapur S, Saluja S, Bhattacharjya S (2016) Material consumption patterns in India. Dtsch. Gesellschaft Für Int. Zusammenarbeit GmbH pp 1–20
19. Shenoy A, Nayak G, Tantri A, Shetty KK (2022) Thermal transmission characteristics of plastic optical fibre embedded light transmitting concrete. Mater Today Proc. https://doi.org/10.1016/j.matpr.2022.04.798
20. CSIR, CSIR—Annual report (2018–19), 2018. https://www.crridom.gov.in/sites/default/files/publication/Annual%20Report%202018-19%20%28English%29.pdf, https://www.crridom.gov.in/publications/reports
21. Kumar M, Prashant S, Kamath MV (2022) Enhancing the sustainability of high strength concrete in terms of embodied energy and carbon emission by incorporating sewage sludge and fly ash. Innov Infrastruct Solut. https://doi.org/10.1007/s41062-022-00837-5
22. Liu S, Minne P, Lulić M, Li J, Gruyaert E (2021) Implementation and validation of Dewar's particle packing model for recycled concrete aggregates. Constr Build Mater. https://doi.org/10.1016/j.conbuildmat.2021.123429
23. Erdem S, Blankson MA (2014) Environmental performance and mechanical analysis of concrete containing recycled asphalt pavement (RAP) and waste precast concrete as aggregate. J Hazard Mater 264:403–410. https://doi.org/10.1016/j.jhazmat.2013.11.040
24. Fournier JM, Álvarez DA, Aenlle AA, Tenza-Abril AJ, Ivorra S (2020) Combining reclaimed asphalt pavement (RAP) and recycled concrete aggregate (RCA) from cuba to obtain a coarse aggregate fraction. Sustainability. https://doi.org/10.3390/su12135356
25. Singh M, Sidddique R, Setia SS, Singh G (2021) Recycling of waste bagasse ash in concrete for sustainable construction. Asian J Civ Eng 22:831–842. https://doi.org/10.1007/s42107-021-00349-0
26. Xiong B, Demartino C, Xu J, Carlo G, Xiao Y (2020) High-strain rate compressive behavior of concrete made with substituted coarse aggregates : recycled crushed concrete and clay bricks.

Constr Build Mater 301:123875. https://doi.org/10.1016/j.conbuildmat.2021.123875
27. Xiao J, Zhang K, Zhang Q (2021) Strain rate effect on compressive stress–strain curves of recycled aggregate concrete with seawater and sea sand. Constr Build Mater 300:124014. https://doi.org/10.1016/j.conbuildmat.2021.124014
28. Nedeljković M, Visser J, Šavija B, Valcke S, Schlangen E (2021) Use of fine recycled concrete aggregates in concrete: a critical review. J Build Eng. https://doi.org/10.1016/j.jobe.2021.102196
29. Patil SV, Balakrishna Rao K, Nayak G (2020) Quality improvement of recycled aggregate concrete using six sigma DMAIC methodology. Int J Math Eng Manag Sci 5:1409–1419. https://doi.org/10.33889/IJMEMS.2020.5.6.104
30. Gonçalves P, De Brito J (2010) Recycled aggregate concrete (RAC): comparative analysis of existing specifications. Mag Concr Res 62:339–346. https://doi.org/10.1680/macr.2008.62.5.339
31. Gencel O, Oguz M, Gholampour A, Ozbakkaloglu T (2021) Recycling waste concretes as fine aggregate and fly ash as binder in production of thermal insulating foam concretes. J Build Eng 38:102232. https://doi.org/10.1016/j.jobe.2021.102232
32. Vavrik WR, Huber G, Pine WJ, Carpenter SH, Bailey R (2002) Bailey method for gradation selection in hot-mix asphalt mixture. Des Transp Res Circ E-C044:34
33. Aurilio V, Pine WJ, Lum P (2005) The Bailey method achieving volumetrics and HMA compactability. In: Fiftieth annual conference of the Canadian technical asphalt association pp 159–183. http://aicms.memexonline.com/dotAsset/89f728e5-6dbb-4d8b-b723-b3f36ecca7d1.pdf
34. Graziani A, Ferrotti G, Pasquini E, Canestrari F (2012) An application to the European practice of the bailey method for HMA aggregate grading design. Proc Soc Behav Sci 53:990–999. https://doi.org/10.1016/j.sbspro.2012.09.948
35. Tantri A, Shenoy A, Nayak G (2021) Characterization of rheological and mechanical properties of self-compacting concrete with Indian standard gradation and particle packing gradations. Springer, Singapore. https://doi.org/10.1007/978-981-15-8293-6_6
36. Tantri A, Nayak G, Shenoy A, Shetty KK (2021) Development of self-compacting concrete using Bailey aggregate grading technique in comparison with Indian standard code of practice. J Eng Des Technol. https://doi.org/10.1108/JEDT-02-2021-0095
37. Tantri A, Nayak G, Kamath M, Shenoy A, Shetty KK (2021) Utilization of cashew nut-shell ash as a cementitious material for the development of reclaimed asphalt pavement incorporated self compacting concrete. Constr Build Mater 301:124197. https://doi.org/10.1016/j.conbuildmat.2021.124197
38. Bahrami N, Zohrabi M, Mahmoudy SA, Akbari M (2020) Optimum recycled concrete aggregate and micro-silica content in self-compacting concrete: Rheological, mechanical and microstructural properties. J Build Eng 31:101361. https://doi.org/10.1016/j.jobe.2020.101361
39. Pu Y, Li L, Wang Q, Shi X, Luan C, Zhang G, Fu L, El-Fatah Abomohra A (2021) Accelerated carbonation technology for enhanced treatment of recycled concrete aggregates: a state-of-the-art review. Constr Build Mater 282:122671. https://doi.org/10.1016/j.conbuildmat.2021.122671
40. Pereira-De-Oliveira LA, Nepomuceno MCS, Castro-Gomes JP, Vila MFC (2014) Permeability properties of self-compacting concrete with coarse recycled aggregates. Constr Build Mater 51:113–120. https://doi.org/10.1016/j.conbuildmat.2013.10.061
41. Grdic ZJ, Toplicic-Curcic GA, Despotovic IM, Ristic NS (2010) Properties of self-compacting concrete prepared with coarse recycled concrete aggregate. Constr Build Mater 24:1129–1133. https://doi.org/10.1016/j.conbuildmat.2009.12.029
42. Fakitsas CG, Papakonstantinou PEA, Kiousis PD, Savva A (2012) Effects of recycled concrete aggregates on the compressive and shear strength of high-strength self-consolidating concrete. J Mater Civ Eng 24:356–361. https://doi.org/10.1061/(asce)mt.1943-5533.0000397
43. Khodair Y, Raza M (2017) Sustainable self-consolidating concrete using recycled asphalt pavement and high volume of supplementary cementitious materials. Constr Build Mater 131:245–253. https://doi.org/10.1016/j.conbuildmat.2016.11.044
44. Shi C, Li Y, Zhang J, Li W, Chong L, Xie Z (2016) Performance enhancement of recycled concrete aggregate: a review. J Clean Prod 112:466–472. https://doi.org/10.1016/j.jclepro.2015.08.057
45. Katz A (2003) Properties of concrete made with recycled aggregate from partially hydrated old concrete. Cem Concr Res 33:703–711. https://doi.org/10.1016/S0008-8846(02)01033-5
46. Katz A (2004) Treatments for the improvement of recycled aggregate. J Mater Civ Eng 16:597–603. https://doi.org/10.1061/(asce)0899-1561(2004)16:6(597)
47. Gómez-Soberón JMV (2002) Porosity of recycled concrete with substitution of recycled concrete aggregate: an experimental study. Cem Concr Res 32:1301–1311. https://doi.org/10.1016/S0008-8846(02)00795-0
48. Tam VWY, Tam CM, Le KN (2007) Removal of cement mortar remains from recycled aggregate using pre-soaking approaches. Resour Conserv Recycl 50:82–101. https://doi.org/10.1016/j.resconrec.2006.05.012
49. Luo J, Chen S, Li Q, Liu C, Gao S, Zhang J, Guo J (2019) Influence of graphene oxide on the mechanical properties, fracture toughness, and microhardness of recycled concrete. Nanomaterials. https://doi.org/10.3390/nano9030325
50. Mohammed SI, Najim KB (2020) Mechanical strength, flexural behavior and fracture energy of recycled concrete aggregate self-compacting concrete. Structures 23:34–43. https://doi.org/10.1016/j.istruc.2019.09.010
51. Kou SC, Poon CS (2010) Properties of concrete prepared with PVA-impregnated recycled concrete aggregates. Cem Concr Compos 32:649–654. https://doi.org/10.1016/j.cemconcomp.2010.05.003
52. Tam VWY, Tam CM (2008) Diversifying two-stage mixing approach (TSMA) for recycled aggregate concrete: TSMAs and TSMAsc. Constr Build Mater 22:2068–2077. https://doi.org/10.1016/j.conbuildmat.2007.07.024
53. Kong D, Lei T, Zheng J, Ma C, Jiang J, Jiang J (2010) Effect and mechanism of surface-coating pozzalanics materials around aggregate on properties and ITZ microstructure of recycled aggregate concrete. Constr Build Mater 24:701–708. https://doi.org/10.1016/j.conbuildmat.2009.10.038
54. Grabiec AM, Klama J, Zawal D, Krupa D (2012) Modification of recycled concrete aggregate by calcium carbonate biodeposition. Constr Build Mater 34:145–150. https://doi.org/10.1016/j.conbuildmat.2012.02.027
55. Spaeth V, Djerbi Tegguer A (2013) Improvement of recycled concrete aggregate properties by polymer treatments. Int J Sustain Built Environ 2:143–152. https://doi.org/10.1016/j.ijsbe.2014.03.003
56. Kou SC, Zhan BJ, Poon CS (2014) Use of a CO2 curing step to improve the properties of concrete prepared with recycled aggregates. Cem Concr Compos 45:22–28. https://doi.org/10.1016/j.cemconcomp.2013.09.008
57. IS: 456 (2000) Concrete, plain and reinforced. Bur Indian Stand Dehli pp 1–114
58. Umamaheswaran K, Batra VS (2008) Physico-chemical characterisation of Indian biomass ashes. Fuel 87:628–638. https://doi.org/10.1016/j.fuel.2007.05.045
59. Munir S, Daood SS, Nimmo W, Cunliffe AM, Gibbs BM (2009) Thermal analysis and devolatilization kinetics of cotton

stalk, sugar cane bagasse and shea meal under nitrogen and air atmospheres. Bioresour Technol 100:1413–1418. https://doi.org/10.1016/j.biortech.2008.07.065
60. Amin M, Zeyad AM, Tayeh BA, Saad Agwa I (2021) Effects of nano cotton stalk and palm leaf ashes on ultrahigh-performance concrete properties incorporating recycled concrete aggregates. Constr Build Mater 302:124196. https://doi.org/10.1016/j.conbuildmat.2021.124196
61. Barbhuiya S, Mukherjee S, Nikraz H (2014) Effects of nano-Al2O3 on early-age microstructural properties of cement paste. Constr Build Mater 52:189–193. https://doi.org/10.1016/j.conbuildmat.2013.11.010
62. ASTM (2010) Standard specification for coal fly ash and raw or calcined natural pozzolan for use. Annu B ASTM Stand pp 3–6. https://doi.org/10.1520/C0618-19.2
63. Diisocyanate T (2006) Standard specification for OPC. Annu B ASTM Stand I pp 1–2. https://doi.org/10.1520/C0150
64. Boudali S, Kerdal DE, Ayed K, Abdulsalam B, Soliman AM (2016) Performance of self-compacting concrete incorporating recycled concrete fines and aggregate exposed to sulphate attack. Constr Build Mater 124:705–713. https://doi.org/10.1016/j.conbuildmat.2016.06.058
65. Sasanipour H, Aslani F, Taherinezhad J (2019) Effect of silica fume on durability of self-compacting concrete made with waste recycled concrete aggregates. Constr Build Mater 227:116598. https://doi.org/10.1016/j.conbuildmat.2019.07.324
66. Revilla-Cuesta V, Ortega-López V, Skaf M, Manso JM (2020) Effect of fine recycled concrete aggregate on the mechanical behavior of self-compacting concrete. Constr Build Mater. https://doi.org/10.1016/j.conbuildmat.2020.120671
67. Omrane M, Rabehi M (2020) Effect of natural pozzolan and recycled concrete aggregates on thermal and physico-mechanical characteristics of self-compacting concrete. Constr Build Mater 247:118576. https://doi.org/10.1016/j.conbuildmat.2020.118576
68. Duan Z, Singh A, Xiao J, Hou S (2020) Combined use of recycled powder and recycled coarse aggregate derived from construction and demolition waste in self-compacting concrete. Constr Build Mater 254:119323. https://doi.org/10.1016/j.conbuildmat.2020.119323
69. IS: 383-2016 (2016) Coarse and fine aggregate for concrete
70. EFNARC (2005) The European guidelines for self-compacting concrete. Eur Guidel Self Compact Concr, p 63. http://www.efnarc.org/pdf/SCCGuidelinesMay2005.pdf
71. IS: 516-1959 (2004) Method of tests for strength of concrete
72. BIS: 5816 (1999) Splitting tensile strength of concrete: method of test
73. IS: 10086-1982 (2008) Indian Standard specification for modulus for use in tests of cement and concrete
74. IS 13311 (Part 1) (1992) Method of non-destructive testing of concret, part 1: ultrasonic pulse velocity. Bur Indian Satandards pp 1–7
75. Santos S, Silva PR, De Brito J (2019) Self-compacting concrete with recycled aggregates: a literature review. J Build Eng 22:349–371. https://doi.org/10.1016/j.jobe.2019.01.001
76. Fiol F, Thomas C, Muñoz C, Ortega-López V, Manso JM (2018) The influence of recycled aggregates from precast elements on the mechanical properties of structural self-compacting concrete. Constr Build Mater 182:309–323. https://doi.org/10.1016/j.conbuildmat.2018.06.132
77. Carro-López D, González-Fonteboa B, De Brito J, Martínez-Abella F, González-Taboada I, Silva P (2015) Study of the rheology of self-compacting concrete with fine recycled concrete aggregates. Constr Build Mater 96:491–501. https://doi.org/10.1016/j.conbuildmat.2015.08.091
78. Kebaïli O, Mouret M, Arabi N, Cassagnabere F (2015) Adverse effect of the mass substitution of natural aggregates by air-dried recycled concrete aggregates on the self-compacting ability of concrete: evidence and analysis through an example. J Clean Prod 87:752–761. https://doi.org/10.1016/j.jclepro.2014.10.077
79. Chakkamalayath J, Joseph A, Al-Baghli H, Hamadah O, Dashti D, Abdulmalek N (2020) Performance evaluation of self-compacting concrete containing volcanic ash and recycled coarse aggregates. Asian J Civ Eng 21:815–827. https://doi.org/10.1007/s42107-020-00242-2
80. Revilla-Cuesta V, Skaf M, Santamaría A, Hernández-Bagaces JJ, Ortega-López V (2021) Temporal flowability evolution of slag-based self-compacting concrete with recycled concrete aggregate. J Clean Prod. https://doi.org/10.1016/j.jclepro.2021.126890
81. Mohammadi Golafshani E, Behnood A, Hosseinikebria SS, Arashpour M (2021) Novel metaheuristic-based type-2 fuzzy inference system for predicting the compressive strength of recycled aggregate concrete. J Clean Prod 320:128771. https://doi.org/10.1016/j.jclepro.2021.128771
82. Rao MC, Bhattacharyya SK, Barai SV (2015) Interfacial transition zone, strength and chloride penetration of recycled aggregate concrete. Indian Concr J 89:54–65
83. Wu J, Zhang Y, Zhu P, Feng J, Hu K (2018) Mechanical properties and ITZ microstructure of recycled aggregate concrete using carbonated recycled coarse aggregate. J Wuhan Univ Technol Mater Sci Ed 33:648–653. https://doi.org/10.1007/s11595-018-1873-1
84. Patil SV, Rao KB, Nayak G (2021) Influence of silica fume on mechanical properties and microhardness of interfacial transition zone of different recycled aggregate concretes. Adv Civ Eng Mater 10:20210011. https://doi.org/10.1520/acem20210011
85. Park WJ, Noguchi T, Shin SH, Oh DY (2015) Modulus of elasticity of recycled aggregate concrete. Mag Concr Res 67:585–591. https://doi.org/10.1680/macr.14.00213
86. Gao Y, Lv SZ, Duan XY, Jia HX, Wu CL (2013) Effect of CFBC fly ash on properties of cement. Wuhan Ligong Daxue Xuebao/J Wuhan Univ Technol 35:17–21. https://doi.org/10.3963/j.issn.1671-4431.2013.04.004
87. Jung SH, Saraswathy V, Karthick S, Kathirvel P, Kwon SJ (2018) Microstructure characteristics of fly ash concrete with rice husk ash and lime stone powder. Int J Concr Struct Mater. https://doi.org/10.1186/s40069-018-0257-4
88. Kamath M, Prashant S, Kumar M (2021) Micro-characterisation of alkali activated paste with fly ash-GGBS-metakaolin binder system with ambient setting characteristics. Constr Build Mater 277:122323. https://doi.org/10.1016/j.conbuildmat.2021.122323
89. Hwang CL, Damtie Yehualaw M, Vo DH, Huynh TP (2019) Development of high-strength alkali-activated pastes containing high volumes of waste brick and ceramic powders. Constr Build Mater 218:519–529. https://doi.org/10.1016/j.conbuildmat.2019.05.143
90. Ishwarya G, Singh B, Deshwal S, Bhattacharyya SK (2019) Effect of sodium carbonate/sodium silicate activator on the rheology, geopolymerization and strength of fly ash/slag geopolymer pastes. Cem Concr Compos 97:226–238. https://doi.org/10.1016/j.cemconcomp.2018.12.007
91. Alarcon-Ruiz L, Platret G, Massieu E, Ehrlacher A (2005) The use of thermal analysis in assessing the effect of temperature on a cement paste. Cem Concr Res 35:609–613. https://doi.org/10.1016/j.cemconres.2004.06.015
92. Zhou Q, Glasser FP (2001) Thermal stability and decomposition mechanisms of ettringite at < 120 °C. Cem Concr Res 31:1333–1339. https://doi.org/10.1016/S0008-8846(01)00558-0
93. Zhang J, Tan H, He X, Zhao R, Yang J, Su Y (2021) Nano particles prepared from hardened cement paste by wet grinding and

its utilization as an accelerator in Portland cement. J Clean Prod 283:124632. https://doi.org/10.1016/j.jclepro.2020.124632
94. Fang X, Xuan D, Zhan B, Li W, Poon CS (2021) A novel upcycling technique of recycled cement paste powder by a two-step carbonation process. J Clean Prod 290:125192. https://doi.org/10.1016/j.jclepro.2020.125192
95. Nonnet E, Lequeux N, Boch P (1999) Elastic properties of high alumina cement castables from room temperature to 1600 °C. J Eur Ceram Soc 19:1575–1583. https://doi.org/10.1016/s0955-2219(98)00255-6
96. Mollah MYA, Kesmez M, Cocke DL (2004) An X-ray diffraction (XRD) and Fourier transform infrared spectroscopic (FT-IR) investigation of the long-term effect on the solidification/stabilization (S/S) of arsenic(V) in Portland cement type-V. Sci Total Environ 325:255–262. https://doi.org/10.1016/j.scitotenv.2003.09.012
97. Péra J, Husson S, Guilhot B (1999) Influence of finely ground limestone on cement hydration. Cem Concr Compos 21:99–105. https://doi.org/10.1016/S0958-9465(98)00020-1
98. Ylmén R, Jäglid U, Steenari BM, Panas I (2009) Early hydration and setting of Portland cement monitored by IR, SEM and Vicat techniques. Cem Concr Res 39:433–439. https://doi.org/10.1016/j.cemconres.2009.01.017
99. Hughes TL, Methven CM, Jones TGJ, Pelham SE, Fletcher P, Hall C (1995) Determining cement composition by Fourier transform infrared spectroscopy. Adv Cem Based Mater 2:91–104. https://doi.org/10.1016/1065-7355(94)00031-X
100. Kloprogge JT, Schuiling RD, Ding Z, Hickey L, Wharton D, Frost RL (2002) Vibrational spectroscopic study of syngenite formed during the treatment of liquid manure with sulphuric acid. Vib Spectrosc 28:209–221. https://doi.org/10.1016/S0924-2031(01)00139-4
101. Trezza MA, Lavat AE (2001) Analysis of the system 3CaO·Al2O3-CaSO4· 2H2O-CaCO3-H2O by FT-IR spectroscopy. Cem Concr Res 31:869–872. https://doi.org/10.1016/S0008-8846(01)00502-6
102. Kristiawan SA, Aditya MTM (2015) Effect of high volume fly ash on shrinkage of self-compacting concrete. Proc Eng 125:705–712. https://doi.org/10.1016/j.proeng.2015.11.110
103. Hanif A, Kim Y, Lu Z, Park C (2017) Early-age behavior of recycled aggregate concrete under steam curing regime. J Clean Prod 152:103–114. https://doi.org/10.1016/j.jclepro.2017.03.107
104. Alnahhal MF, Alengaram UJ, Jumaat MZ, Abutaha F, Alqedra MA, Nayaka RR (2018) Assessment on engineering properties and CO2 emissions of recycled aggregate concrete incorporating waste products as supplements to Portland cement. J Clean Prod 203:822–835. https://doi.org/10.1016/j.jclepro.2018.08.292
105. Hill N, Walker H, Beevor J, James K (2011) Guidelines to defra/DECC's GHG conversion factors for company reporting: methodology paper for emission factors contents, p 102. https://assets.publishing.service.gov.uk/government/uploads/system/uploads/attachment_data/file/69314/pb13625-emission-factor-methodology-paper-110905.pdf